Available online at www.sciencedirect.com

ScienceDirect

Geochimica et Cosmochimica Acta 284 (2020) 222–238

Geochimica et Cosmochimica Acta

www.elsevier.com/locate/gca

Constraining speleothem oxygen isotope disequilibrium driven by rapid CO_2 degassing and calcite precipitation: Insights from monitoring and modeling

Peter E. Carlson [a,*], Alexandra L. Noronha [a], Jay L. Banner [a], John W. Jenson [b], Mark W. Moore [a], Judson W. Partin [c], Michael Deininger [d], Daniel O. Breecker [a], Kaylyn K. Bautista [b]

[a] *Jackson School of Geosciences, University of Texas at Austin, 78712, USA*
[b] *Water and Environmental Research Institute of the Western Pacific, University of Guam, Mangilao, GU 96923, USA*
[c] *Institute for Geophysics, Jackson School of Geosciences, University of Texas at Austin, Austin, TX 78758, USA*
[d] *Institute of Geosciences Johannes Gutenberg University Mainz, J.-J.-Becher-Weg 21, 55128 Mainz, Germany*

Received 15 February 2020; accepted in revised form 11 June 2020; Available online 25 June 2020

Abstract

Oxygen isotopes are the most commonly applied speleothem proxy for reconstructing Quaternary changes in precipitation and/or temperature. These interpretations are either limited to qualitative wetting and drying trends or rely on theoretical, experimental and/or empirical equilibrium isotope fractionation factors for more quantitative constraints. These various fractionation factors have similar temperature sensitivities, but their absolute values differ, and cave calcite does not appear to generally precipitate in isotopic equilibrium with its drip water. Rapid CO_2 degassing paired with calcite precipitation, both occurring under disequilibrium conditions, are a set of mechanisms commonly invoked to explain offsets between observed and equilibrium isotopic fractionation between cave calcites and drip waters. However, the relevance of these disequilibrium mechanisms to speleothem records remains unresolved. Here, we compare measured $\delta^{18}O$ values of modern speleothem calcite from a tropical cave in Guam to calcite $\delta^{18}O$ values predicted by a modified version of the ISOLUTION proxy system model. This extends the global comparison of cave drip water and modern calcite $\delta^{18}O$ values to higher temperatures. We initialize the model using contemporaneous measurements of drip water ($\delta^{18}O$ values, [Ca^{+}], and pH), and cave air (CO_2, and T) from four drip sites over 3.5 years of monitoring in the cave. Through this comparison, we show that for a slow drip-rate site, ventilation-driven CO_2 degassing can explain seasonal variations in calcite oxygen isotope composition. At faster-dripping sites in this cave, the seasonal effect is limited. At these sites, the DIC reservoir is replenished by new drips faster than its isotopic composition can be modified by degassing CO_2 and calcite precipitation, whether occurring each is occurring as an equilibrium or kinetic process. For the slow drip rate site, however, this is the first observation of cave air CO_2 variations exerting a control on cave calcite oxygen isotope values. The confirmation of ventilation-driven processes controlling oxygen isotope values at a slow-drip site advances the process-based understanding of stalagmite formation that is required to move beyond the wetter-or-drier paradigm and make quantitative interpretations of speleothem oxygen isotope records.

Keywords: Speleothems; Paleoclimatology; Oxygen isotopes (δ18O); Proxy system model; ISOLUTION

* Corresponding author at: Jackson School of Geosciences, 2305 Speedway Stop C1160, Austin, TX 78712, USA.
E-mail address: PeterCarlson@utexas.edu (P.E. Carlson).

https://doi.org/10.1016/j.gca.2020.06.012
0016-7037/

1. INTRODUCTION

The issue of whether calcite-water oxygen isotope fractionation in cave calcite can be described by isotope equilibrium has long challenged quantitative interpretations of speleothem oxygen isotope records. Although early experimental attempts to determine calcite-water oxygen isotope equilibrium fractionation values (e.g., O'Neil et al., 1969; Friedman and O'Neil, 1977; Kim and O'Neil, 1997) showed good agreement with early theoretical models (e.g., Chacko and Deines, 2008), measurements of cave calcite-water oxygen isotope fractionation diverged strongly from these predictions of equilibrium (e.g., Mickler et al. 2004, 2006; Tremaine et al., 2011; Daëron et al., 2019). This discrepancy between speleothem measurements and calculated isotopic equilibrium has led researchers to question both the assumption of equilibrium isotopic fractionation in cave calcite precipitation (Mickler et al., 2006; Daëron et al., 2019), as well as the validity of accepted equilibrium values (Coplen, 2007; Daëron et al., 2019). Recent laboratory studies of calcite precipitating slowly from thin films (Polag et al., 2010; Day and Henderson, 2011; Affek and Zaarur, 2014) or on seed crystals in a chemostatic solution (Levitt et al., 2018) and of well-dated and very slow-growing subaqueous calcite (Coplen et al., 2007; Daëron et al., 2019) suggest that the commonly used experimental values, determined by precipitating calcite from bulk solution (e.g. Kim and O'Neil, 1997), are not applicable to the vast majority of speleothems and point to the existence of rate-dependent, disequilibrium fractionation effects in both natural systems and laboratory settings. In this study, we use the term "disequilibrium fractionation" after Deininger and Scholz (2019) to collectively describe the processes resulting in calcite deposited on stalagmites that is not in oxygen isotope equilibrium with its corresponding drip water at the time of drip impact on the speleothem surface. This is an important distinction for speleothem paleoclimate studies, because the immediate objective for most is to reconstruct drip water oxygen isotope values from speleothem calcite oxygen isotope values. The disequilibrium fractionation processes that can interfere with these reconstructions include kinetic isotope effects (as traditionally defined by O'Neil et al., 1969) and open system, Rayleigh-type processes (e.g., CO_2 degassing, evaporation, and calcite precipitation) which may or may not involve equilibrium isotope fractionation, but have the potential to alter the oxygen isotope composition of the dissolved inorganic carbon (DIC) reservoir from which the calcite precipitates.

The inability to constrain the degree to which isotope fractionation (equilibrium or disequilibrium) is driven by site-specific effects such as cave or speleothem geometry, drip rates, or climate adds uncertainty to the interpretation of speleothem $\delta^{18}O$ records that is difficult to quantify. Recent laboratory precipitation experiments and theoretical models predict a dependence of calcite-water oxygen isotope fractionation factors on calcite growth rate and pH (e.g., Watkins et al., 2013, 2014; Devriendt et al., 2017; Hansen et al., 2019). The predicted dependence is that higher calcite growth rates result in pH-dependent kinetic isotope effects and non-equilibrium calcite-water oxygen isotope fractionation, and slower growth rates allow for pH-independent isotope fractionation nearer to equilibrium values (DePaolo, 2011; Watkins et al., 2014). The effect of calcite growth rate on calcite-water oxygen isotope fractionation is often invoked in the literature to explain observed offsets between cave calcite $\delta^{18}O$ values and those expected for equilibrium with drip water (e.g. Johnston et al., 2013, Stoll et al., 2015). Stoll et al. (2015) demonstrated good agreement between five speleothem calcite $\delta^{18}O$ records when adjusted for growth-rate-dependent calcite-water oxygen isotope fractionation, but did not report differences between calcite and water $\delta^{18}O$ values.

Calcite precipitation modeling can inform interpretations of isotope disequilibrium, but pairing calcite growth rate models to isotopic models is nontrivial. Dreybrodt (2008) described two models of isotope evolution during calcite precipitation: (1) a continuous-flow model (FLOW; Romanov et al., 2008) where calcite grown near the drip axis is in near oxygen-isotope equilibrium with the dripping water and (2) a stagnant pool model, where DIC in a static pool of water on the speleothem surface undergoes Rayleigh distillation before being replenished by the next drip. The latter situation has been extensively modeled (Hendy, 1971; Dreybrodt and Scholz, 2011; Deininger et al., 2012; Owen et al., 2018; Deininger and Scholz, 2019) and, to a lesser extent, used to explain carbon and oxygen isotope values of speleothems (Bar-Matthews et al., 1996; Mickler et al. 2004, 2006, 2019). Watkins et al. (2014) modeled calcite-DIC oxygen isotope fractionation factors as a function of the growth rate, rather than as a function of the drip rate, using an ion-by-ion crystal growth model that distinguishes between the attachment and detachment of carbonate and bicarbonate ions to and from the crystal surface, as well as the oxygen-isotope composition of each. Most recently, Guo and Zhou (2019) published a reaction–diffusion model of carbonate precipitation, tracking the forward and reverse reaction rates of the (de)hydroxylation of bicarbonate and of the (de)hydration of carbonic acid in the water film for each isotopologue of the two DIC species.

Here, we use the results of seven years of monitoring at Jinapsan Cave, Guam, including calcite grown on glass substrates at four sites with growth rates ranging from 0.05-20 mg/day, to test a model of oxygen isotope fractionation in cave drip waters (ISOLUTION; Dieninger et al., 2012, Dieninger and Scholz, 2019). This tropical cave is an ideal site to consider CO_2-degassing-driven and growth-rate-driven disequilibrium fractionation, because the minimally variable annual temperature (25.7–27.8 °C; Noronha et al., 2017) and constant high humidity (95–100% RH; Partin et al., 2012) of the tropical cave allow us to confidently ignore temperature- and evaporation-driven effects on calcite-water oxygen isotope fractionation. Furthermore, growth-rate-driven changes in fractionation due to surface entrapment of ^{16}O during calcite precipitation are largest at higher temperatures (Watson and Liang, 1995; Watson, 1996, 2004; Dietzel et al., 2009; Day and Henderson, 2011), and Jipansan Cave has a relatively high temperature (~26 °C).

2. SITE DESCRIPTION

The island of Guam (13.4 °N, 144.5 °E) is the largest and southernmost island in the Mariana Islands volcanic arc. Guam lies within the West Pacific Warm Pool and receives 2000–2500 mm of rainfall annually over distinct wet and dry seasons, with ~70% of annual precipitation occurring during the July-December wet season (Lander and Guard, 2003). The dry season is characterized by persistent northeasterly trade winds, with most rain falling as light showers. The wet season begins when the trade winds slacken, and typically shift southeastward, resulting in more humid and unstable atmospheric conditions over the island. Formation of convective clouds drive moderate to heavy downpours, which are responsible for the majority of wet-season precipitation (Lander et al., 2001). Wet-season precipitation is also affected by tropical cyclone activity, with ~30% of Guam's wet-season precipitation induced by tropical cyclones (Kubota and Wang, 2009).

The northern half of the island comprises an uplifted carbonate plateau containing numerous caves. Jinapsan Cave is a small progradational collapse cave (Miklavič, 2011) located on the northernmost point of the island, near Ritidian Point. The cave is located within 500 m of the beach in limestone forest, an ecological classification accounting for 34% of the land surface of Guam, described by thin, calcic soils and tall >10 m broadleaf trees of mixed species (Donnegan et al., 2004). The cave has a single restricted opening, which is the highest point of the cave, and consists of a single chamber, though large flowstones and stalagmites form walls, which give the illusion of multiple rooms (Bautista et al., 2018). Mean daily cave air temperature is 27 °C and is constant throughout the year. Because of its tropical location, this cave does not undergo the temperature-driven seasonal ventilation observed in temperate-latitude caves (Wigley and Brown, 1976; Buecher, 1999; James et al., 2015). Instead, seasonal variation in the direction and magnitude of the trade winds drives ventilation of Jinapsan Cave, with high ventilation and low cave pCO_2 Dec-Jun, and low ventilation and high cave pCO_2 Jun-Dec (Noronha et al., 2017).

Four drip sites are considered in this study: Flatman, Station 1, Station 2, and Stumpy (See Fig. 1 of Partin et al., 2012; Bautista et al., 2018). Drip water $\delta^{18}O$ values from each site, from July 2008 to November 2010, have been previously reported by Partin et al. (2012), and extended to 2015 by Beal et al. (2018). Drip water chemical composition has been reported by Noronha et al. (2017) and Beal et al. (2018), and calcite deposition rates at these sites have been reported by Noronha et al. (2017). The first of these sites, Flatman, is located in a pseudo-chamber (Midslide, 188 m^3) 12.0 m below the cave entrance and 24.2 m below the ground surface (Bautista et al., 2018). The second and third drip sites, Station 1 and Station 2, are located 1 m from each other in a smaller pseudo-chamber (Shakey Room, 11 m^3), slightly deeper in the cave, off of the main descent. These sites are 23.5 and 24.5 m below the cave entrance, and 27.5 and 28.5 m below the ground surface, respectively (Bautista et al., 2018). Drip site Station 2 fed the stalagmite referred to in Sinclair et al. (2012) as "Big Guam" or "Shakey" before its collection for analysis. The final drip site considered in this study, Stumpy, is in an even deeper pseudo-chamber of the cave (Stumpy Room, 16 m^3) connected to the Shakey Room of Stations 1 and 2. This site is 27.8 m below the entrance, and 34 m below the ground surface (Bautista et al., 2018). The Stumpy drip site fed the "Little Guam" or "Stumpy" stalagmite reported by Sinclair et al. (2012). Hourly cave pCO_2 measurements, reported by Noronha et al. (2017), were taken near site Stumpy.

3. METHODS

3.1. Cave Sample Collection

Sampling of cave drip water at Jinapsan Cave began in early 2008, was established as a routine monthly collection

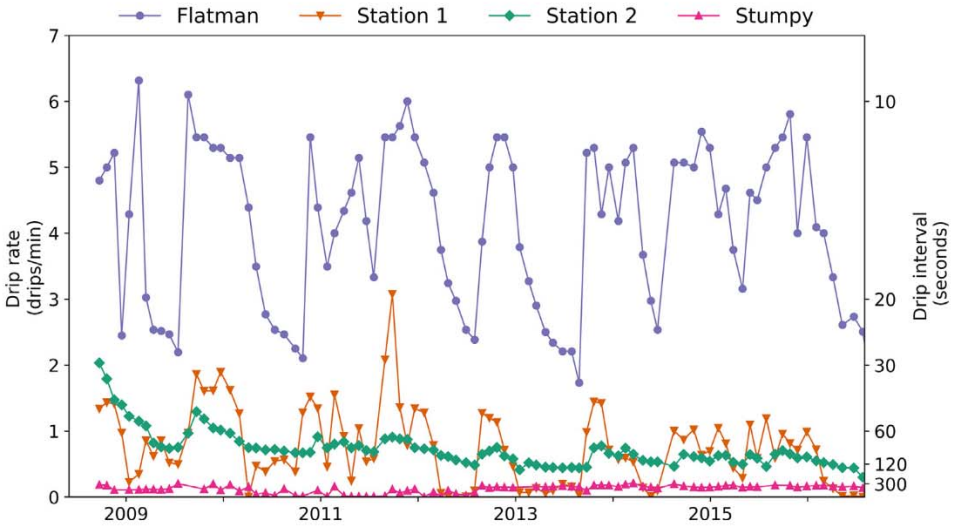

Fig. 1. Measurements of drip interval and calculated drip rates for drip sites Flatman, Station 1, Station 2, and Stumpy. First reported by Noronha et al. (2017). Higher drip rates (shorter drip intervals) correspond to increased water flux, whereas lower drip rates (longer drip intervals) correspond to decreased water flux.

program in August 2008, and was completed in September 2016. Samples were collected at seven drip sites and the cave pool during this period (Partin et al., 2012, Noronha et al. 2017, Beal et al., 2018). Results are reported in this study from samples collected at four of the sites: Flatman, Station 1, Station 2, and Stumpy. The monthly monitoring program included collection of water and drip rate data and calcite grown on glass substrates at all sites, and deployment/collection of loggers that recorded continuous cave air CO_2 concentrations, temperature, barometric pressure, and relative humidity at site Stumpy.

Drip water was collected in pre-weighed wide-mouthed HDPE Nalgene bottles that were deployed under the drip and left for ~24 hours. Collection bottles were weighed and water was decanted into bottles in the cave and pretreated for a suite of geochemical analyses. Aliquots of drip water for $\delta^{18}O$ measurement were stored in 4 mL glass dram vials with no headspace. These aliquots were refrigerated until analysis, with the exception of the time spent in transit from University of Guam to the University of Texas at Austin. Aliquots of drip water for analysis of cation concentrations were stored in acid-washed 30 mL HDPE Nalgene bottles and preserved with 60 µL of Seastar nitric acid. When sufficient water remained after these aliquots had been decanted, pH, conductivity, and water temperature were measured using a Myron Ultrameter II – 6P (Myron L Company, Carlsbad, CA, USA).

Calcite was grown on 10 × 10 cm glass plates that were frosted using glass beads to facilitate calcite nucleation. Glass substrates were weighed with a Sartorius MCI RC 210P electronic balance (Sartorius, Goettingen, Germany) before and after deployment in the cave to determine calcite growth rate. A standard plate was weighed to reduce variability in plate weight measurements associated with static electricity, humidity, and other environmental variables, following the methods established by Banner et al. (2007). Glass substrates were left in place for 3–12 weeks and were removed and replaced during 24-hour water collection period. In January 2012, PVC holders for the glass substrates were installed under each drip site to ensure consistent plate orientation.

3.2. Cave Environmental Measurements

Cave CO_2 concentration was measured at 1-hour intervals using a Vaisala GM70 CO_2 probe (0–5000 ppm measurement range) and a Vaisala M170 data logger (Vaisala Corp, Helsinki, Finland). Beginning in 2012, the CO_2 logging assembly was deployed in a modified Pelican dry box (Pelican Products, Inc., Torrance, CA, USA) with ~ 500 g of desiccant (W.A. Hammond Drierite Co. Ltd., Xenia, OH, USA) or generic vermiculite to avoid condensation at high humidity. Measurement errors associated with this probe are CO_2-dependent, at ± (2% of the reading + 75 ppm CO_2), or ± 80–175 ppm CO_2 in measured cave conditions. CO_2 measurements in supersaturated air are considered unreliable due to water condensation. Cave air temperature, pressure, and relative humidity were logged at 1-hour intervals using HOBO Micro-Station Data Loggers (HOBO, Onset, Bourne, MA, USA), with measurement errors of ±0.21 °C, ±5% RH and ±3.0 mbar, respectively.

Drip rates (drips per minute) were measured monthly and calculated by measuring the time elapsed between drips. Standard protocol was to measure the interval between four consecutive drips three times and to report the average of these measurements as the drip interval (seconds). When the drip interval exceeded 300 seconds, the long drip interval was noted, but no measurement of drip interval was taken.

3.3. Stable Isotope Analysis

A total of 140 glass substrate calcite samples (Flatman, n = 35; Station 1, n = 32; Station 2, n = 41; Stumpy, n = 32) and 278 drip water samples were analyzed (Flatman, n = 62; Station 1, n = 82; Station 2, n = 72; Stumpy, n = 62) for carbon and oxygen stable isotope ratios. All stable isotope analyses were carried out in facilities at the University of Texas at Austin (UT). New water $\delta^{18}O$ measurements presented in this manuscript were analyzed on a Thermo-Finnigan MAT-253 equipped with a Gas Bench II via CO_2 equilibration at the UT Stable Isotope Lab for Critical Zone Gases. For each measurement, 1 mL of water was added to 12 mL LabCo Exetainer vials which are sealed and purged with 0.3% CO_2 in He and equilibrated at 40°C for 8 hours. Results are normalized based on replicate measurements of internal laboratory standards calibrated on the VSLAP-VSMOW scale with a long-term analytical precision of ± 0.2‰ (2σ). Methods used for previously-published water $\delta^{18}O$ measurements considered in this manuscript are described by Partin et al. (2012).

The $\delta^{18}O$ values of glass substrate calcite samples were measured using a Thermo-Finnigan MAT-253 equipped with a Gas Bench II or a Thermo-Finnigan Delta V equipped with Kiel IV device. Approximately 300 µg of calcite was collected from the center of the glass substrate with a scalpel and transferred to 12 mL LabCo Exetainer vials. Vials were flushed with He, and calcite samples were converted to CO_2 via reaction with 103% H_3PO_4 for 2 hours at 50 °C. Delta values were normalized to the PDB scale using a two-point calibration (NBS-18 and NBS-19 IAEA standards), following a correction for run drift with an internal standard of Cararra marble. Fifteen samples were analyzed in the UT Analytical Laboratory for Paleoclimatic Studies on a Thermo Finnigan Delta V equipped with Kiel IV device using 30–50 µg of calcite using the methods described by Partin et al. (2012).

3.4. Data Analysis

Calcite-water oxygen isotope fractionation factors are calculated using the measured $\delta^{18}O_{calcite}$ for each glass substrate and the average of all $\delta^{18}O_{water}$ measurements made at the corresponding site while the substrate was deployed. In cases where measured drip interval is unavailable, drip interval is calculated from the mass of water collected, using a density of 1.0 g/mL, and the mean drip volume of all sites (0.07 mL). All drip water, calcite, and model results are reported in Electronic Annex Tables A1 and A2.

3.5. Fractionation Calculations

Calcite-water oxygen isotope fractionation can be reported using one of two commonly used expressions. The per mil fractionation factor $1000ln(\alpha)$ (Eqs. (1)–(2)), is an exact form, reserved for theoretically, empirically, or experimentally derived equilibrium fractionation relationships. The alternative, $\Delta^{18}O_{c-w}$ (Eq. (3)), is inexact, but commonly used to report observed fractionations, whether or not they represent isotope equilibrium. In this paper, $\Delta^{18}O_{c-w}$ will be used for comparisons among the observations made in this study. The exact form, $1000ln(\alpha)$, will be used for comparisons with published calcite-water oxygen isotope equilibrium relationships. Throughout the paper, measurements of calcite $\delta^{18}O$ will be reported in per mil on the Peedee Belemnite scale (‰ PDB) and measurements of water $\delta^{18}O$ will be reported in per mil on the Vienna Mean Standard Ocean Water scale (‰ VSMOW). When direct comparisons are made between water and calcite $\delta^{18}O$ values, the water $\delta^{18}O$ values will first be converted to PDB. All $\delta^{13}C$ values are reported in ‰ PDB.

$$per\ mil\ fractionation\ factor = 1000\ ln(\alpha) \tag{1}$$

$$\alpha = \frac{1000 + \delta^{18}O_{calcite}}{1000 + \delta^{18}O_{water}} \tag{2}$$

$$\text{Fractionation} \approx \Delta^{18}O_{c-w} = \delta^{18}O_{calcite} - \delta^{18}O_{water} \tag{3}$$

3.6. Modeling

Two different model treatments, "Equilibrium" and "ISOLUTION," were compared. In the simplistic Equilibrium treatment, the reservoir of water for each calcite sample was treated as a static reservoir of water with a fixed oxygen isotope composition. In this treatment, the oxygen isotope composition of calcite depends only on the oxygen isotope composition of the drip water, the water temperature, and the calibration chosen for calcite-water oxygen isotope equilibrium: either Kim and O'Neil (1997), Coplen (2007), or Affek and Zaarur (2014).

The ISOLUTION treatment is more complex, accounting for oxygen isotope fractionating processes associated with calcite precipitation between drips (Deininger et al., 2012; Deininger and Scholz, 2019). To model the degree of oxygen isotope disequilibrium fractionation occurring on the stalagmite surface between drips, we used the ISOLUTION proxy system model introduced by Deininger et al. (2012). This model is initialized by equilibrating water with calcite and estimated or measured soil CO_2 concentrations, and allowing the water to drip onto a speleothem surface, where it partially displaces pre-existing water, degasses CO_2, evaporates, and precipitates calcite before it is partially displaced by the next drip. Theoretical equilibrium Ca^{2+} concentrations were determined using PHREEQC (Parkhurst and Appelo, 1999), with measured cave CO_2 concentrations, measured cave air temperature, and, due to water sample volume limitations, the mean of measured drip water pH (8.0 ± 0.5) as inputs. To calculate calcite deposition rates, ISOLUTION (Deininger et al., 2012; Deininger and Scholz, 2019) was modified to accept measured drip-water $[Ca^{2+}]$ rather than soil CO_2 concentrations (Eqs. (4)–(6); Dreybrodt et al., 1998; Noronha et al., 2017) and to use the calcite growth rate constant α_p from Hansen (2013; Eq. (4)), where dt is seconds between drips, δ is water film thickness, chosen to be 0.0001 meters (Noronha et al., 2017).

$$Growth\ \ Rate\left[\frac{g}{day}\right] = W_o\left[\frac{g}{m^2 \cdot s}\right] \cdot 86400\left[\frac{s}{day}\right] \cdot \frac{V_{drop}[m^3]}{\delta[m]} \tag{4}$$

$$W_o\left[\frac{g}{m^2 \cdot s}\right] = (Ca_{meas} - Ca_{equil})\left[\frac{g}{m^3}\right] \cdot \frac{\delta[m]}{dt[s]} \cdot (1 - e^{\frac{-\alpha_p[m/s]}{\delta[m]} \cdot dt[s]}) \tag{5}$$

$$\alpha_p\left[\frac{m}{s}\right] = (0.52\left[\frac{m}{s}\right] + 0.04\left[\frac{m}{s \cdot K}\right] \cdot T[K] + 0.004\left[\frac{m}{s \cdot K^2}\right] \cdot T[K]^2) \cdot 10^{-5}) \tag{6}$$

ISOLUTION assumes that the water film is static between drips. The DIC pool is assumed to be in chemical and isotope equilibrium with the H_2O pool before CO_2 degassing begins. It is then altered by CO_2 degassing, which forces a chemical disequilibrium between the DIC pool and the cave atmosphere, leading to calcite precipitation. Both CO_2 degassing and calcite precipitation alter DIC $\delta^{18}O$ values from the original values of the DIC pool, in turn affecting the $\delta^{18}O$ values of the precipitated calcite. We also note that CO_2 degassing is accompanied by the dehydration of carbonic acid and the dehydroxylation of bicarbonate, both of which remove oxygen from the DIC pool. The ISOLUTION model considers CO_2 degassing as an isotope equilibrium process. Although both CO_2 degassing and its associated processes and calcite precipitation pull the DIC pool out of oxygen isotope equilibrium with the H_2O pool, further oxygen isotope exchange is not considered between the H_2O and DIC pools. ISOLUTION allows for evaporation to concentrate the DIC pool, but evaporation rates at Jinapsan cave were assumed to be negligible, as humidity in this cave is $\sim 100\%$ (Partin et al., 2012). In this study, calcite-water oxygen isotope fractionation relationships following the calibrations of Kim and O'Neil (1997), Affek and Zaarur (2014), or Coplen (2007) were used for the calcite-water oxygen isotope fractionation step of the ISOLUTION calculations. Although we do not assume that calcite precipitates in oxygen isotope equilibrium with H_2O, these fractionation factors are useful for determining calcite-bicarbonate oxygen isotope fractionation factors (Table 1) (see Fig. 2).

It is also worth noting that although ISOLUTION can model oxygen isotope disequilibrium, it does not explicitly model kinetic isotope effects (KIE), the subset of disequilibrium isotope effects caused by differences in forward and reverse reaction rates (O'Neil et al., 1969; Kim et al., 2006; Dietzel et al., 2009; Gabitov et al., 2012; Watkins et al., 2013, 2014; Sade and Halevy, 2017; Chen et al., 2018; Guo and Zhou, 2019). Each individual reaction modeled by ISOLUTION uses equilibrium fraction factors. Instead, oxygen isotope disequilibrium effects between calcite and drip water in ISOLUTION arise from Rayleigh fractionation of the bulk DIC pool (combined carbonate,

Table 1
Oxygen Isotope Per Mil Fractionation Factors used in the Modified ISOLUTION Code.

Empirical: Fractionation Steps

	Fractionation Steps*	1000*lnα Equation*	1000*lnα* (@ 26 °C)	Citation
A	$H_2O_{(l)} \rightarrow HCO_{3(aq)}^-$	$\frac{-2.59 \cdot 10^6}{T^2} - 1.89$	−30.86	Beck et al., 2005
B	$CO_{2(aq)} \rightarrow H_2O_{(l)}$	$\frac{2.52 \cdot 10^6}{T^2} + 12.12$	40.31	Beck et al., 2005
C	$CO_{2(g)} \rightarrow CO_{2(aq)}$	$-1000 \ln\left(\left(\frac{-1605150}{T^2} + \frac{1441.76}{T} - 1.9585\right)/1000 + 1\right)$	−1.07	Thorstenson and Parkhurst, 2004
D_1	$CaCO_{3(s)} \rightarrow H_2O_{(l)}$	$\frac{1.803 \cdot 10^4}{T} - 32.42$	27.88	Kim and O'Neil, 1997
D_2	$CaCO_{3(s)} \rightarrow H_2O_{(l)}$	$\frac{1.74 \cdot 10^4}{T} - 28.6$	29.59	Coplen, 2007
D_3	$CaCO_{3(s)} \rightarrow H_2O_{(l)}$	$\frac{1.563 \cdot 10^4}{T} - 23.29$	28.98	Affek and Zaarur, 2014

Derived: Reaction Products

	Reaction Products + Steps*	1000*lnα Equation*	1000*lnα* (@ 26 °C)
E_1	$CaCO_{3(s)} \rightarrow HCO_{3(aq)}^-$	$A + D_1$	−2.98
E_2	$CaCO_{3(s)} \rightarrow HCO_{3(aq)}^-$	$A + D_2$	−1.27
E_3	$CaCO_{3(s)} \rightarrow HCO_{3(aq)}^-$	$A + D_3$	−1.88
F	$CO_{2(g)} \rightarrow HCO_{3(aq)}^-$	$A + B + C$	8.38

*Derived: Bulk Product***

	Reaction Components (O-Containing Molecules)	1000*lnα Equation*	1000*lnα* (@ 26 °C)
G_1	$CO_{2(g)} + CaCO_{3(s)} + H_2O_{(l)} \rightarrow HCO_{3(aq)}^-$	$1000ln\left(\frac{2}{6}e^{\left(\frac{F}{1000}\right)} + \frac{3}{6}e^{\left(\frac{E_1}{1000}\right)} + \frac{1}{6}e^{\left(\frac{A}{1000}\right)}\right)$	−3.75
G_2	$CO_{2(g)} + CaCO_{3(s)} + H_2O_{(l)} \rightarrow HCO_{3(aq)}^-$	$1000ln\left(\frac{2}{6}e^{\left(\frac{F}{1000}\right)} + \frac{3}{6}e^{\left(\frac{E_2}{1000}\right)} + \frac{1}{6}e^{\left(\frac{A}{1000}\right)}\right)$	−2.90
G_3	$CO_{2(g)} + CaCO_{3(s)} + H_2O_{(l)} \rightarrow HCO_{3(aq)}^-$	$1000ln\left(\frac{2}{6}e^{\left(\frac{F}{1000}\right)} + \frac{3}{6}e^{\left(\frac{E_3}{1000}\right)} + \frac{1}{6}e^{\left(\frac{A}{1000}\right)}\right)$	−3.20

* These steps do not imply balanced chemical reactions but are instead useful oxygen isotope equilibrium relationships that may have several intermediate chemical steps.

** Combined oxygen-bearing products of CO_2 degassing-driven calcite precipitation: Calcite, water, and gaseous CO_2. 1000ln(α) for bulk product – bicarbonate is weighted by mole fraction of oxygen in the bulk product.

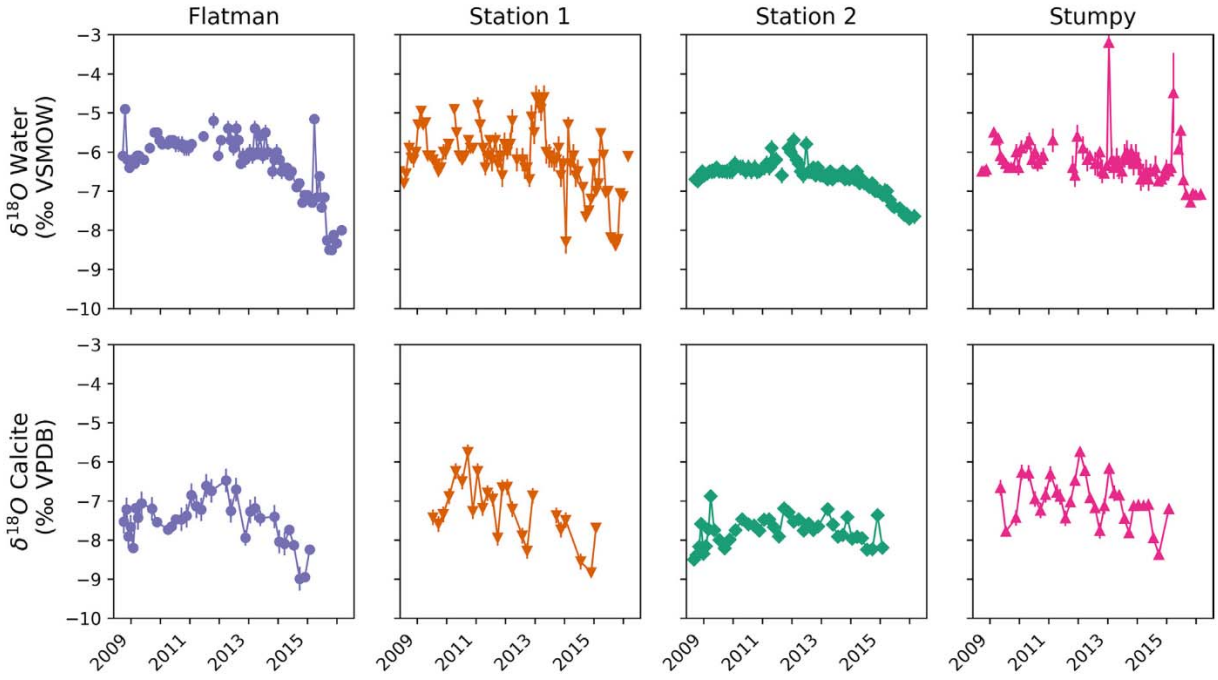

Fig. 2. Measurements of drip water and calcite $\delta^{18}O$. Measurement uncertainty is shown as vertical error bars (1σ). In each case, the multi-year trend of the drip water signal is recorded in the calcite.

bicarbonate, and carbonic acid) as oxygen atoms are removed through CO_2 degassing and calcite precipitation. Although the lack of KIE modeling in ISOLUTION is a serious limitation of the model, explicit KIE modeling would also require modeling reaction rates for each step of the process, would double the number of fractionation

factors, and significantly increase the complexity and computational demand of the model, while eliminating the easy comparison to the widely-used calcite-water oxygen isotope equilibrium fractionation factors examined here.

4. RESULTS

4.1. Drip Rate Measurements

The four drip sites considered here represent a range of drip rates and drip rate variabilities (Noronha et al., 2017; Fig. 1). For better comparison among disparate drips, we report the mean, standard deviation, range, and coefficient of variability (CV). The fastest dripping site, Flatman, has a mean drip rate of 4.11 ± 1.23 drips/min (range 1.58–6.32; CV 0.30) over the monitored period (autumn 2008-summer 2016). The slowest drip site, Stumpy, has a mean drip rate of 0.12 ± 0.06 drips/min (range 0.00–0.21; CV 0.43). The two intermediate sites, Stations 1 and 2, have similar mean drip rates of 0.76 ± 0.57 drips/min (range 0.00–3.08; CV 0.75) and 0.73 ± 0.28 drips/min (range 0.30–2.03; CV 0.27).

Three of the four drip sites showed significant drying or wetting trends. The most significant of these is a drying trend observed at Station 2 ($p = 2 \times 10^{-15}$; Wald Test). When this trend was removed, the CV of the detrended drip rates at Station dropped from 0.39 to 0.27. While a similar drying trend was observed at Station 1 ($p = 2 \times 10^{-3}$), removing the trend had less of an effect on CV, lowering it from 0.75 to 0.71. Similarly, at Stumpy, removing a slight wetting trend ($p = 4 \times 10^{-4}$) decreased CV from 0.48 to 0.43. No significant trend was observed at site Flatman.

4.2. Drip Water and Calcite $\delta^{18}O$ Measurements

Multi-year trends in the measured drip water $\delta^{18}O$ values are recorded in the measured substrate calcite $\delta^{18}O$ values, but seasonal signals in drip water $\delta^{18}O$ values are not as closely recorded in substrate calcite (Fig. 2) and are therefore less likely to be accurately translated into the speleothem record. The calcite $\delta^{18}O$ record may contain a seasonal component not observed in the drip-water $\delta^{18}O$ record (Station 2, Stumpy) or miss high-amplitude, short-duration excursions observed in the drip-water $\delta^{18}O$ record (Flatman, Station 1).

Because drip water was collected multiple times (typically 2 or 3) during each calcite growth period, drip water $\delta^{18}O$ measurements were averaged to directly compare them to calcite $\delta^{18}O$ values. When compared in this way (Fig. 3), we find strong correlations between averaged drip water and calcite $\delta^{18}O$ values for Stumpy ($r^2 = 0.45$; $p = 2 \times 10^{-4}$), Station 1 ($r^2 = 0.55$; $p = 6 \times 10^{-4}$), and Flatman ($r^2 = 0.64$; $p = 9 \times 10^{-3}$), and a weak correlation at Station 2 ($r^2 = 0.17$; $p = 5 \times 10^{-2}$). Station 2 also has a lower slope ($m = 0.66 \pm 0.23$) than Station 1 ($m = 1.28 \pm 0.24$) or Stumpy ($m = 1.40 \pm 0.30$). Flatman has an intermediate slope ($m = 01.01 \pm 0.13$) that cannot be distinguished from the higher or lower slopes. In all cases, significance is calculated from Pearson's r with autoregression-corrected effective degrees of freedom v_{eff} (after Hu et al., 2017).

The relationships between the drip water $\delta^{18}O$ signals and the calcite $\delta^{18}O$ records can be further examined by calculating the oxygen isotope fractionation ($\Delta^{18}O_{c-w}$) between each calcite-water pair (Fig. 4). These $\Delta^{18}O_{c-w}$ values range from 27.79 to 29.95 ‰ PDB, with a mean near the per mil equilibrium fractionation factors predicted by

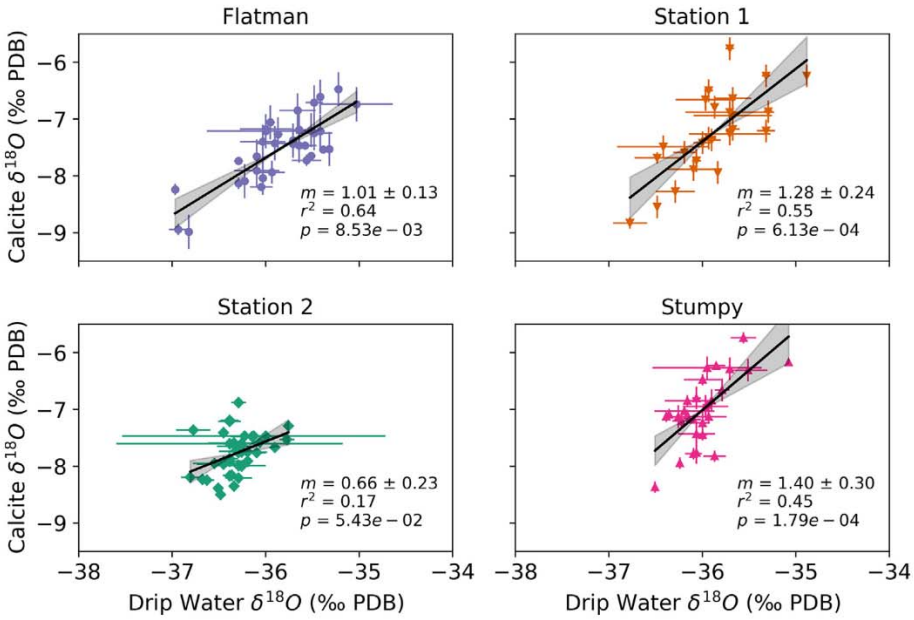

Fig. 3. Calcite $\delta^{18}O$ values plotted against the average of drip water $\delta^{18}O$ values over each calcite growth period for the four drip sites in this study. Measurement uncertainty (1 σ) for calcite is shown as vertical error bars. Standard deviations of multiple drip water measurements from the same calcite growth period are shown as horizontal error bars. Best fit lines (least squares) are shown in black, with 90% confidence bands of the best fit lines in gray.

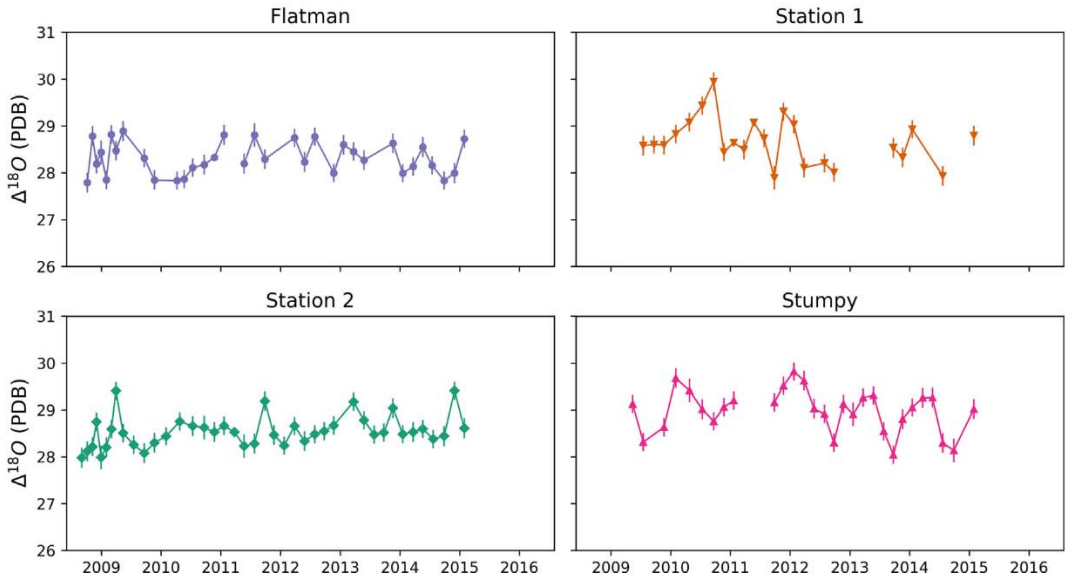

Fig. 4. $\Delta^{18}O_{c-w}$ (Eq. (3)) values calculated using averaged drip water and calcite $\delta^{18}O$ values, in ‰ PDB. Drip $\delta^{18}O$ values are averaged from 1-3 measurements taken during the calcite growth period (2 months) for a corresponding calcite $\delta^{18}O$ measurement. Vertical bars represent 1σ uncertainty.

Coplen (2007), Tremaine et al. (2011), and Affek and Zaarur (2014), but significantly higher than the per mil fractionation factors predicted by Kim and O'Neil (1997) over the temperature range of measured drip water (26.5 ± 0.5 °C; 2σ) (Fig. 5). These data also extend the body of compiled cave calcite-water oxygen isotope fractionation factors (e.g., McDermott et al., 2006; 2011; Tremaine et al., 2011; Johnston et al., 2013) to warmer temperatures (Fig. 5).

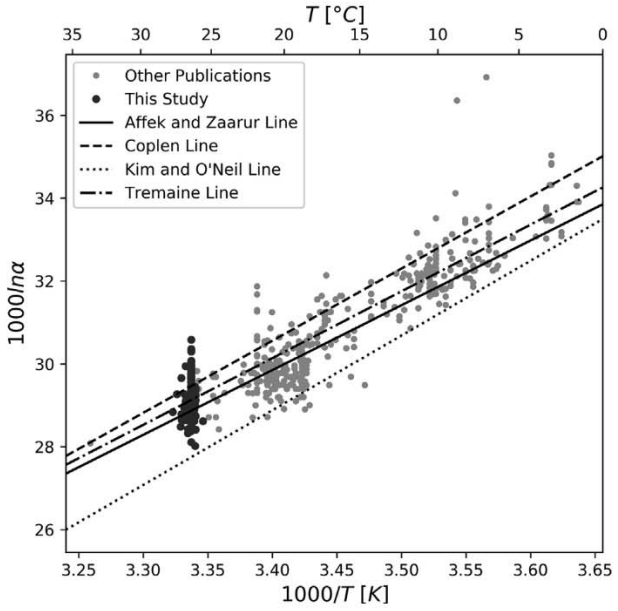

Fig. 5. Per mil fractionation factors calculated using averaged values of drip water $\delta^{18}O$, calcite $\delta^{18}O$, and drip water (where available) or cave air temperature for 370 cave calcite records compiled from 56 studies (gray circles) and this study (black circles). Oxygen isotope equilibrium fractionation as calculated in Coplen (2007; dashed line), Tremaine et al. (2011; dash-dot line), Affek and Zaarur (2014; solid line) and Kim and O'Neil (1997; dotted line) is also shown. To see records plotted by study, see Electronic Annex Fig. A1 and Electronic Annex Table A3.

When we compare $\Delta^{18}O_{c-w}$ to drip rate at all sites, we find a significant negative relationship ($r^2 = 0.21$; $p = 4 \times 10^{-8}$), with faster drip rates associated with lower $\Delta^{18}O_{c-w}$ values, and slower drip rates associated with a range from low to high $\Delta^{18}O_{c-w}$ values (Fig. 6). Correlations within drip sites were less significant, with only Stumpy ($r^2 = 0.17$; $p = 3 \times 10^{-2}$) and Station 2 ($r^2 = 0.18$; $p = 5 \times 10^{-3}$) showing significant correlations between drip rate and $\Delta^{18}O_{c-w}$ values.

We find a similarly low, but still significant, correlation ($r^2 = 0.19$; $p = 1 \times 10^{-6}$) between $\Delta^{18}O_{c-w}$ and calcite deposition rate (determined by weighing glass substrates), with larger deposition rates associated with smaller $\Delta^{18}O_{c-w}$. For this comparison, we calculate a molar growth rate constant R_c (μmol calcite/m^2/hr), assuming even calcite growth on a 100 ± 6 cm^2 glass substrate (Eq. (7)). The slope of the observed $\Delta^{18}O_{c-w}$ – log(R_c) relationship is −0.32 ± 0.06 (90% confidence; Fig. 6), which is within the ranges of the slopes observed in both field (–0.9 to 0.0; Feng et al., 2012) and laboratory studies (–1.1 to −0.3; Dietzel et al., 2009; Hansen et al., 2019). No site showed an independently significant correlation between $\Delta^{18}O_{c-w}$ and log(R_c).

$$Rc = \frac{\text{grams calcite}}{\text{hours deployed}} \cdot \left(\frac{1E-2\ m^2}{\text{plate}}\right)^{-1} \cdot \left(\frac{100.09\ \text{grams calcite}}{\text{mol calcite}}\right)^{-1} \cdot \frac{1E6\ \mu\text{mol}}{\text{mol}} \quad (7)$$

4.3. Calcite $\delta^{13}C$ Measurements

Stable carbon isotope compositions ($\delta^{13}C$) of the calcite correlate with $\delta^{18}O$ values (Fig. 7). The slopes (m) of the

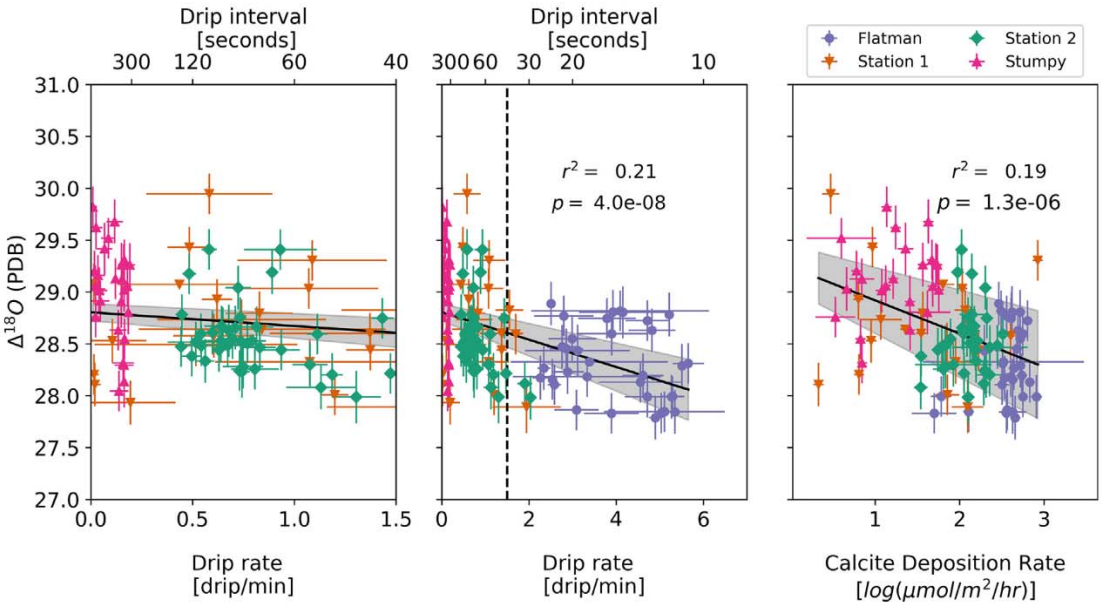

Fig. 6. $\Delta^{18}O_{c-w}$ (Eq. (3)) values versus drip rate (drip/min; left, center) and calcite deposition rate log(R_c; right), where R_c is μmol calcite/m^2/hr on a 100 ± 6 cm^2 glass substrate. In all panels, gray region shows the 90% confidence interval of the best fit line. The left panel shows a detailed view of portion of the center panel that lies to the left of the vertical dashed line. Vertical and horizontal bars represent 1σ uncertainty.

regression lines between calcite $\delta^{13}C$ and $\delta^{18}O$ values at site Stumpy ($m = 1.95 \pm 0.25$) and site Station 2 ($m = 2.11 \pm 0.26$) were the highest, with Station 1 only slightly lower ($m = 1.37 \pm 0.41$) and Flatman, the site with the highest drip rate, significantly lower ($m = 0.69 \pm 0.22$). All correlations were highly significant ($p < 0.01$). Because $\delta^{13}C$ values of drip water DIC were not measured in this study, and likely varied through time, the ISOLUTION model could not be properly initialized for $\delta^{13}C$ calculations, and the simulated $\delta^{13}C$ values were ignored.

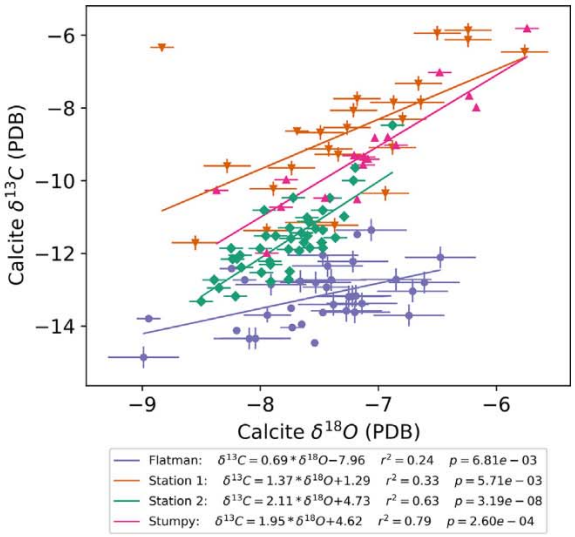

Fig. 7. Substrate calcite $\delta^{13}C$ versus $\delta^{18}O$ values at each drip site, with associated regressions, r^2 values, and p values. In the legend, sites are listed in approximate descending order of drip rate, from Flatman (fastest drip rate) to Stumpy (slowest drip rate). Stations 1 and 2 have similar long-term drip rate averages, but drip rates are more variable at Station 1 than at Station 2.

4.4. Modeled Calcite $\delta^{18}O$ Results

The two model treatments (equilibrium and ISOLUTION) combined with three empirical equilibrium fractionation relationships (Kim and O'Neil, 1997; Coplen, 2007; Affek and Zaarur, 2014) define six model variations. Each model variation produced predicted calcite $\delta^{18}O$ values that moderately, but significantly correlated to measured calcite $\delta^{18}O$ values, with r^2 values between 0.2 and 0.29, and p values ranging from 2.66×10^{-14} to 3.27×10^{-18} (Fig. 8). Of the six model variations, disequilibrium-fractionation-enabled using Affek and Zaarur (2014) (Affek-Zaarur/ISOLUTION) best predicts our measured calcite $\delta^{18}O$ values, with a root mean square error (RMSE) of 0.42‰ and a mean offset of –0.13‰ between modeled and measured calcite $\delta^{18}O$. The Coplen/Equilibrium model (RMSE = 0.51‰; offset = 0.22‰) better fits the data than either the Affek and Zaarur/Equilibrium (RMSE = 0.59‰; offset = –0.37‰) or Kim and O'Neil/Equilibrium (RMSE = 1.56‰; offset = –1.49‰) models, or the Coplen/ISOLUTION (RMSE = 0.59‰; offset = 0.44‰) and Kim and O'Neil/ISOLUTION (RMSE = 1.27 ‰; offset = –1.20‰) models.

For the Affek-Zaarur/ISOLUTION model, differences between the model and measured/empirical $\Delta^{18}O_{c-w}$ values vary significantly by drip site (Fig. 9). Whereas the Affek-Zaarur/ISOLUTION model does not significantly improve predictions at Flatman, the site with the highest drip rates, it significantly outperforms the Affek-Zaarur/Equilibrium

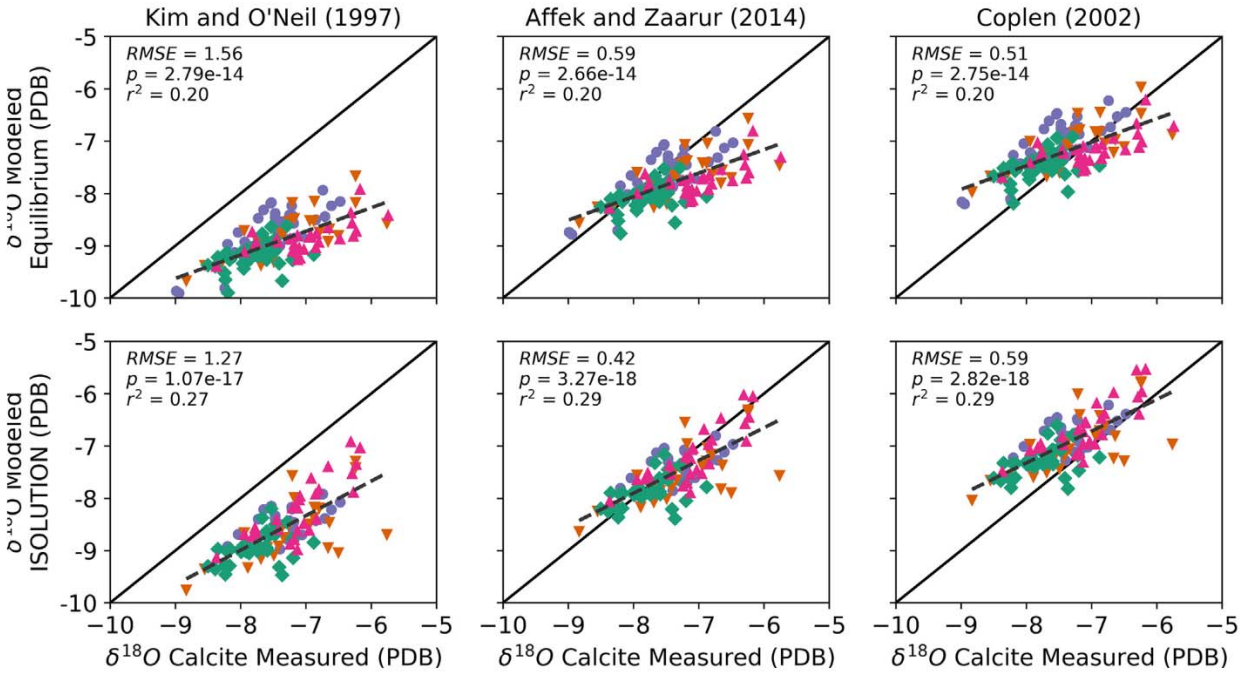

Fig. 8. Modeled versus measured calcite $\delta^{18}O$ values for the four Jinapsan cave speleothems. The first column of panels uses Kim and O'Neil (1997) for calcite-water oxygen isotope equilibrium. The second column uses Affek and Zaarur (2014) and the third uses Coplen (2007). The top row of panels is modeled assuming isotopic equilibrium with calcite is precipitated from an isotopically static DIC reservoir. The second row is modeled using ISOLUTION, which also assumes oxygen isotope equilibrium fractionation, but accounts for the changing isotopic composition of the DIC reservoir as CO_2 degasses and calcite precipitates.

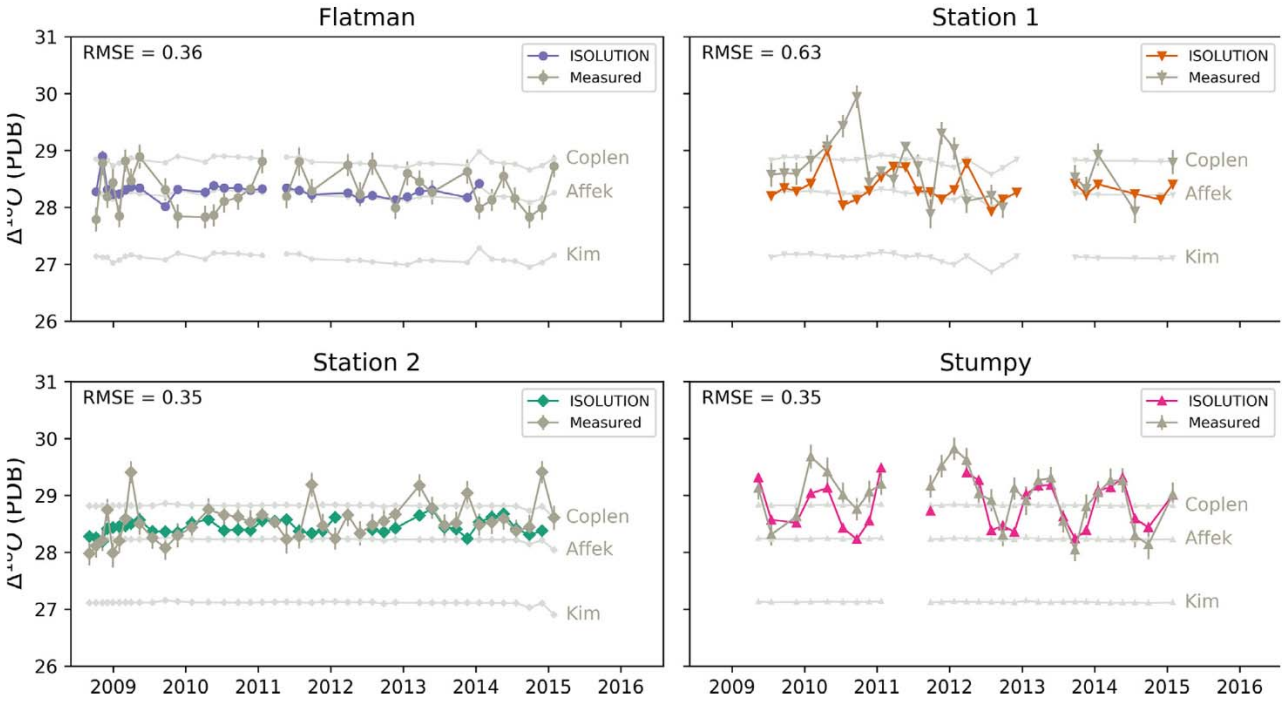

Fig. 9. Comparison between modeled and empirical $\Delta^{18}O_{c-w}$ values. Each panel shows (1) Equilibrium $\Delta^{18}O_{c-w}$ values (light gray lines and symbols, labeled by study), (2) ISOLUTION-modeled $\Delta^{18}O_{c-w}$ values using Affek and Zaarur (2014) for equilibrium fractionation and estimated isotope disequilibrium fractionation (colored lines and symbols), and (3) the observed $\Delta^{18}O_{c-w}$ values (dark gray lines and symbols). Vertical lines represent 1σ uncertainty in measured $\Delta^{18}O_{c-w}$ values. The ISOLUTION model significantly out-performs equilibrium fractionation for the site with the lowest drip rate (Stumpy) and moderate drip rates (Stations 1 and 2) but does not significantly improve predictions at the high drip-rate site (Flatman). Of the moderate drip rate sites, the ISOLUTION model performs better in the site with less drip rate variability (Station 2).

model for Stumpy, the site with the slowest drip rate. At sites with intermediate drip rates, Stations 1 and 2, inclusion of the ISOLUTION model does address some of the temporal variability of $\Delta^{18}O_{c-w}$ values. Accounting for processes that might result in lack of oxygen isotope equilibrium between calcite and H_2O on stalagmites explains the seasonality observed in $\Delta^{18}O_{c-w}$ values at Stumpy, especially after 2012, the year field measurements of CO_2 concentrations at this site improved.

5. DISCUSSION

5.1. Controls on calcite-water oxygen isotope fractionation

Although temperature is the primary control on calcite-water oxygen isotope fractionation factors used by speleothem scientists (Urey, 1947; McCrea, 1950; O'Neil et al., 1969; Friedman and O'Neil, 1977; Kim and O'Neil, 1997; Tremaine et al., 2011; Affek and Zaarur, 2014), the low variability in drip-water temperatures observed in Jinapsan Cave (Noronha et al., 2017; Fig. 5; Electronic Annex Table A1) rule out temperature variability as the primary control on $\Delta^{18}O_{c-w}$ variability at this site.

We find first that (A) $\Delta^{18}O_{c-w}$ negatively correlates to both drip rate and calcite deposition rate (Fig. 6), and (B) that these relationships are driven by variability between drip sites, rather than within drip sites. The first observations are consistent with CO_2-degasing-driven isotope disequilibrium fractionation (Mickler et al., 2004; Mühlinghaus et al., 2007; Deininger et al., 2012), as slower drip rates allow for greater alterations of the DIC pool before the pool is replenished by the next drip, and because calcite deposition rates are significantly controlled by drip rates. The second observation might be explained by the $\sim$ 30-day resolution of our drip rate monitoring, which is better-suited to characterize differences between drip sites than to capture ephemeral changes in drip rates in a single site.

In the ion-by-ion model proposed by Watkins et al. (2014), higher $\Delta^{18}O_{c-w}$ values are generally representative of less growth-rate-induced kinetic fractionation, whereas lower $\Delta^{18}O_{c-w}$ values are characteristic of more growth-rate-induced kinetic fractionation. In both the Watkins et al. (2014) ion-by-ion model and the Watson (2004) bicarbonate surface entrapment model, departure from equilibrium fractionation is represented by decreasing $\Delta^{18}O_{c-w}$ values. These models, combined with the higher fractionation factors they assume, are therefore a possible alternative explanation for some of our results in Jinapsan Cave, as well as for calcite-water oxygen isotope fractionation observed in other cave settings (e.g., Feng et al., 2012; see also Daëron et al., 2019). These models cannot, however, explain fractionation factors observed to fall above the Coplen (2007) equilibrium line (33 of 133 samples in this study; Fig. 9).

5.2. Using ISOLUTION to Test the Importance of Rayleigh Fractionation

ISOLUTION models Rayleigh fractionation of the bulk DIC pool to predict calcite $\delta^{18}O$ values from input drip water $\delta^{18}O$ values, drip water physicochemical parameters, and cave environmental parameters. The success of this model varied significantly by drip rate and drip rate variability, better predicting $\Delta^{18}O_{c-w}$ values at slower and less variable drip sites (Fig. 9, Fig. 6).

At the fast drip-rate site (Flatman; 4.11 ± 1.23 drips/min, 1σ), the model performed no better than a simplistic isotopic equilibrium model, but at the slow drip-rate site (Stumpy; 0.12 ± 0.06 drips/min, 1σ), the model successfully explained both observed $\Delta^{18}O_{c-w}$ values and $\Delta^{18}O_{c-w}$ variability. At the fast drip rate site, the modeled water reservoir is replenished before significant alteration of the DIC pool can occur, whereas at the slow drip site, the water film may remain un-replenished for minutes at a time, during which CO_2-degassing and calcite precipitation can pull the DIC pool away from its original $\delta^{18}O$ values: CO_2-degassing by increasing, and calcite precipitation by decreasing, the $\delta^{18}O$ values of the remaining DIC pool.

At the intermediate drip-rate sites (Station 1, 0.76 ± 0.57 drips/min, 1σ; and Station 2, 0.73 ± 0.28 drips/min, 1σ), the modified ISOLUTION model predicts a portion, but not all, of the observed $\Delta^{18}O_{c-w}$ variability. This could be explained by variability in drip rates, drip $\delta^{18}O$ values, or $[Ca^{2+}]$ values not captured by monthly drip monitoring, or by sources of kinetic fractionation and disequilibrium that were not considered in this model, such as the pH-dependent fractionation accounted for in the ion-by-ion model (Watkins et al., 2014). Unidentified species in solution, like organic molecules or other metals, can also influence calcite deposition rates and growth habits (e.g., Inskeep and Bloom 1986; Granit, et al., 2003; Ihli, et al., 2016; Innocenti Malini et al., 2017; Tang et al., 2019), and thereby possibly affect $\Delta^{18}O_{c-w}$ values (Watson, 2004; DePaolo, 2011).

At the intermediate and slow drip rate sites, measured $\Delta^{18}O_{c-w}$ values significantly exceeded equilibrium $\Delta^{18}O_{c-w}$ values predicted by Coplen et al. (2007; Fig. 9). Assuming Coplen et al. (2007) represents a close approximation of calcite-water oxygen isotope equilibrium, these values cannot be explained by KIE alone, which decrease fractionation factors compared to equilibrium. The inclusion of Rayleigh fractionation, which increases fractionation factors in this system, allows ISOLUTION to model $\Delta^{18}O_{c-w}$ values in excess of Coplen equilibrium.

5.3. Seasonal variability of $\Delta^{18}O_{c-w}$ values

At the Stumpy drip site, there is a clear seasonal variability in $\Delta^{18}O_{c-w}$ values. Because drip rate and drip $\delta^{18}O$ variability are not seasonal at this site, we consider the seasonality in $\Delta^{18}O_{c-w}$ variability at Stumpy to be driven primarily by seasonality of cave air CO_2 concentrations (Fig. 10). The Stumpy site and, to a lesser extent, Station 1 and Station 2, are located in a small, partially-enclosed section on the periphery of the cave (Partin et al., 2012; Bautista et al., 2018) that is poorly ventilated, except during the dry season when the trade winds are strong (Noronha et al., 2017). Seasonal variations in cave air CO_2 concentrations mimic $\Delta^{18}O_{c-w}$ shifts. We suggest that during intervals of high CO_2, less CO_2 degassing occurs, driving less

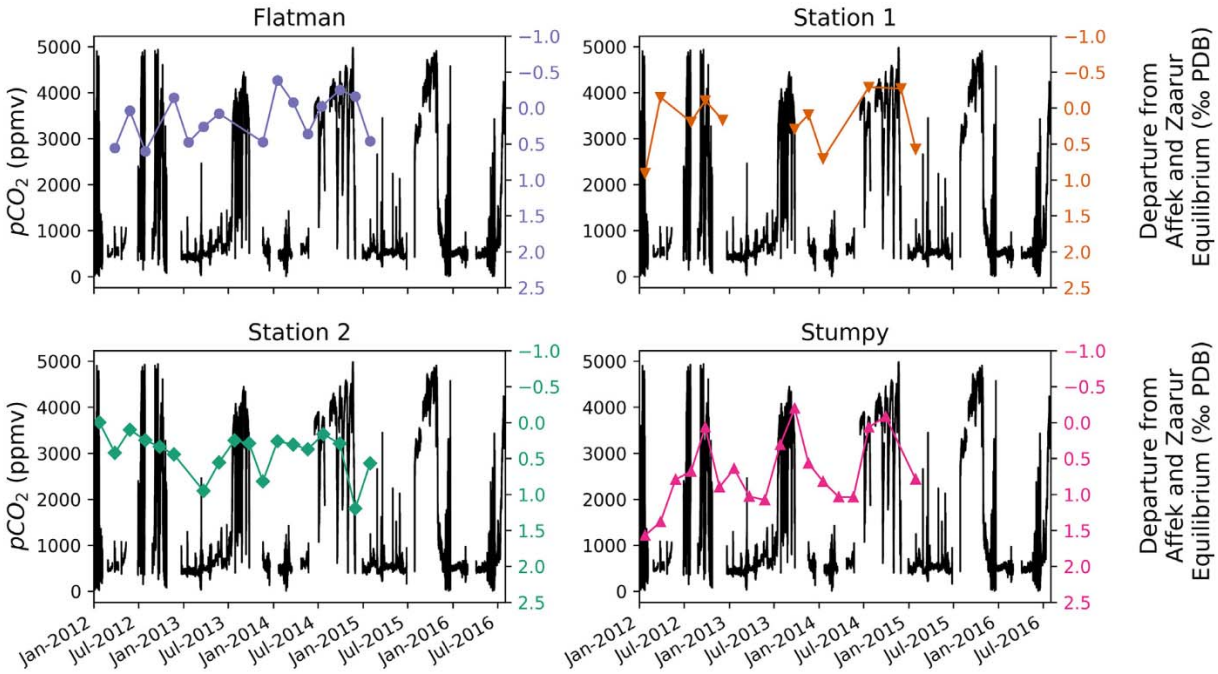

Fig. 10. Daily average Jinapsan cave CO_2 concentrations (black dots; logger measured near site Stumpy; Noronha et al., 2017) and the difference between measured $\Delta^{18}O_{c-w}$ and Affek and Zaarur (2014) equilibrium 1000ln(α) for substrate calcite at all four drip sites (colored symbols and lines) for the period of well-constrained CO_2 measurements (post-3/26/2012; Noronha et al., 2017). Note that the y-axis is reversed for $\Delta^{18}O_{c-w}$. During this period, greater departures from Affek and Zaarur (2014) equilibrium are observed to coincide with periods of low cave air CO_2. This is particularly evident at sites Stumpy and Station 1, less-so at site Station 2, and not observed at site Flatman. During periods of low cave air CO_2, more drip-water degassing of CO_2 will occur, increasing the degree of alteration of the DIC reservoir from its original $\delta^{18}O$ values. See Electronic Annex Fig. A.2 for a comparison of monthly CO_2 measurements taken near Flatman and near Stations 1 and 2 to the hourly CO2 measurements recorded near Stumpy.

alteration of the DIC pool from its original $\delta^{18}O$ values (Deininger et al., 2012; Deininger and Scholz, 2019) and thus calcite is precipitated with $\delta^{18}O$ values closer to equilibrium with water. This is the first demonstration, to our knowledge, of an effect of cave CO_2 concentrations on cave calcite $\delta^{18}O$. This effect occurs to at a lesser degree at the faster-drip sites Station 1, Station 2, and Flatman (Fig. 10), which are also located in more well-ventilated areas of the cave. A comparison of monthly CO_2 measurements taken near Flatman and near Stations 1 and 2 to the hourly CO_2 measurements recorded near Stumpy is reserved for the Electronic Annex (Electronic Annex Fig. A.2). Our results indicate that the processes resulting in isotope disequilibrium fractionation are more important at the site that is variably ventilated and has slow drip rates, consistent with ISOLUTION sensitivity studies (Deininger et al., 2012).

5.4. Seasonal Variability in $\delta^{13}C$ Values

Although practical limitations of this study did not allow us to measure $\delta^{13}C$ values of drip water DIC, and thereby properly initialize ISOLUTION for carbon isotope modeling, variations in measured substrate calcite $\delta^{13}C$ are consistent with CO_2-degassing-driven isotope disequilibrium fractionation at slower drip sites. It has long been understood that certain processes leading to isotope disequilibrium fractionation can exert similar controls over speleothem $\delta^{18}O$ and $\delta^{13}C$ values (see Hendy, 1971; Desmarchelier et al., 2000; Mickler et al., 2004; Mickler et al., 2006). Rapid degassing of CO_2 with relatively low $\delta^{13}C$ and $\delta^{18}O$ values can increase $\delta^{13}C$ and $\delta^{18}O$ values of the remaining DIC from which calcite may eventually precipitate. Given constant initial DIC oxygen- and carbon-isotope compositions, this effect would be greatest at sites with slower drip rates, and during periods with lower cave-air CO_2 (Mickler et al., 2006). Although constant initial DIC $\delta^{13}C$ values cannot be confirmed at these sites, comparisons between substrate calcite $\delta^{13}C$ values and cave air CO_2 concentrations (Fig. 11) generally show increases in calcite $\delta^{13}C$ values coincident with periods of low CO_2. This relationship is clearest at the slower drip-rate sites Station 1, Station 2, and Stumpy.

5.5. Covariation of Calcite $\delta^{13}C$ and $\delta^{18}O$ Values

Examining the best-fit slope (m) of measured calcite $\delta^{13}C$ versus $\delta^{18}O$ values at a given drip site can provide additional context to the results of the ISOLUTION model (Fig. 7). Specifically, these slopes can provide a qualitative estimate of the degree of oxygen isotope buffering between the drip water and the drip water DIC pools, a process by which changes in the $\delta^{18}O$ values of the DIC pool are reversed by complete or partial equilibration with the much

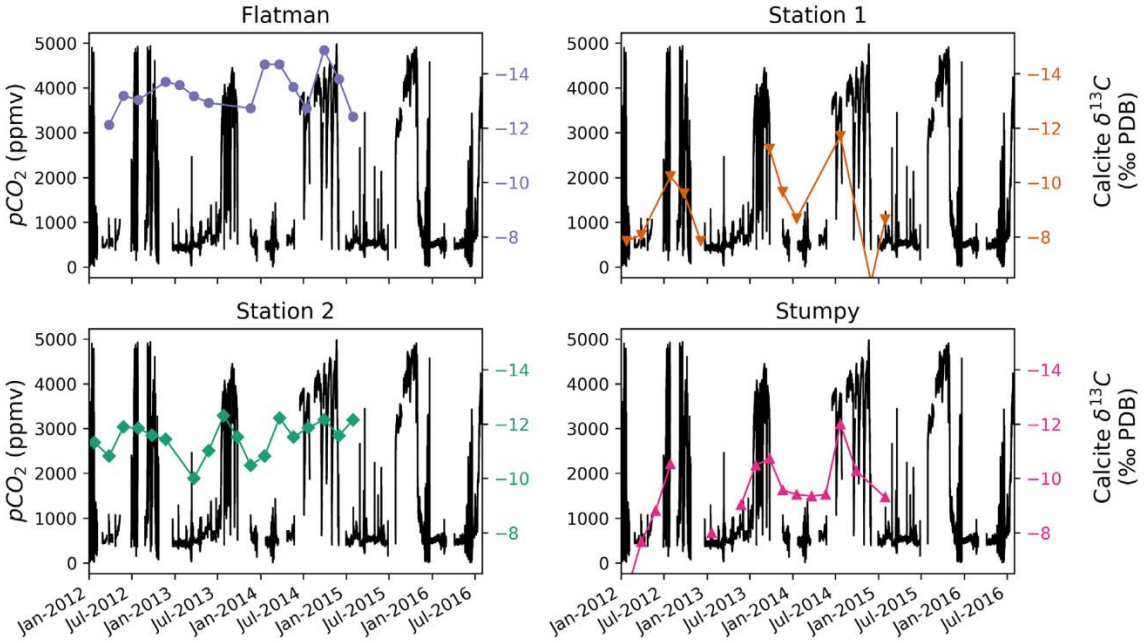

Fig. 11. Daily average Jinapsan cave air CO_2 concentrations (black dots; logger located near site Stumpy; Noronha et al., 2017) and substrate calcite $\delta^{13}C$ values at all four drip sites (colored symbols and lines) for the period of well-constrained CO_2 measurements (post-3/26/2012; Noronha et al., 2017). Note that the y-axis is reversed for $\delta^{13}C$. During this period, larger calcite $\delta^{13}C$ values are generally observed during periods of low cave air CO_2. This is particularly evident at the slower drip sites Stumpy and Station 1, less-so at site Station 2, and not observed at the fastest drip site Flatman.

larger (in terms of total O atoms) H_2O pool. This process, which is currently unaccounted for in the ISOLUTION model, can alter calcite and DIC $\delta^{18}O$ values without altering $\delta^{13}C$ values. For speleothem samples with no $\delta^{18}O$ buffering between the H_2O reservoir and the DIC reservoir, Mickler et al. (2006) calculate a theoretical calcite $\delta^{13}C$–$\delta^{18}O$ slope of 0.52 at 26.1 °C. This slope increases with the degree of H_2O-DIC $\delta^{18}O$ buffering. In a fully H_2O-buffered system, CO_2 degassing will only alter DIC and calcite $\delta^{13}C$ values, and the calcite $\delta^{13}C$-$\delta^{18}O$ slope will be vertical. As the hydration/dehydration and hydroxylation/dehydroxylation reactions that allow for this buffering occur on timescales (hours to days for HCO_3^--dominated solutions; see Watkins et al., 2013) longer than typical drip rates at monitored drip sites and longer than typical CO_2-degassing rates (seconds to minutes; Dreybrodt and Scholz, 2011; Hansen et al., 2013), partial H_2O-DIC $\delta^{18}O$ buffering is expected. As drip rates increase, the water residence time (and, hence, the time for buffering) will decrease, and the slope of the $\delta^{13}C$-$\delta^{18}O$ relationship will decrease, approaching 0.5.

The best-fit slopes m between substrate calcite $\delta^{13}C$ and $\delta^{18}O$ reported for each site (Fig. 7; Flatman, $m = 0.69$; Station 1, $m = 1.37$; Station 2, $m = 2.11$; Stumpy, $m = 1.95$) are consistent with the theoretical CO_2-degassing-driven $\delta^{13}C$-$\delta^{18}O$ slopes determined by Mickler et al. (2006) for samples with intermediate H_2O-DIC $\delta^{18}O$ buffering. The site with the fastest drip rate (Flatman) is consistent with the least H_2O-DIC $\delta^{18}O$ buffering of all four sites, followed by Station 1. When combined with the conflicting observation that the ISOLUTION model was least able to predict calcite $\delta^{18}O$ values at Flatman and Station 1 (Fig. 9), this suggests: (A) H_2O-DIC $\delta^{18}O$ buffering is not a dominant control of calcite $\delta^{18}O$ values at these sites, and (B) there likely exists a "Goldilocks" range of drip rates for the application of the current ISOLUTION model. With drip rates that are too fast, not enough CO_2 degassing can occur to significantly alter the $\delta^{18}O$ values of the DIC pool (as observed at site Flatman), and calcite $\delta^{18}O$ variability may instead be dominated by unmeasured variability in drip water $\delta^{18}O$ values. With drip rates that are significantly slower than observed in this study, H_2O-DIC $\delta^{18}O$ buffering may minimize or prevent entirely changes to the $\delta^{18}O$ values of the DIC pool, a process not currently accounted for in ISOLUTION.

5.6. Limitations of the modified ISOLUTION Model

We find four primary limitations to the ISOLUTION model. First, as discussed above, this model does not consider H_2O-DIC oxygen exchange as a potential mechanism for altering DIC $\delta^{18}O$ values over the residence time of the drip. Because the sum effect of the processes considered by ISOLUTION (i.e., CO_2 degassing, CO_2 (de)hydration, bicarbonate (de)hydroxylation, and calcite precipitation) is an oxygen-atom-weighted per mil bulk fractionation factor of –3.03‰ at 30 °C (between $HCO_{3(aq)}$ and the reaction products $CO_{2(g)}$, $H_2O_{(l)}$, and $CaCO_{3(s)}$), the overall effect of CO_2 degassing and calcite precipitation is to increase $\delta^{18}O$ values of the remaining DIC pool. Ignoring H_2O-DIC $\delta^{18}O$ buffering therefore causes ISOLUTION to overestimate modeled calcite $\delta^{18}O$ values.

Second, the ISOLUTION model treats the CO_2 degassing step as a process occurring in isotope equilibrium that has a relatively small per mil fractionation factor of −1.05‰. In cave conditions, however, CO_2 degassing may be a kinetic process with a significantly more negative per mil fractionation factor (Mickler et al., 2004; Affek and Zaarur, 2014; Mickler et al., 2019). The assumption of equilibrium CO_2 degassing, therefore, may cause an underestimation of modeled calcite $\delta^{18}O$ values, opposite the effect expected from unmodeled H_2O-DIC $\delta^{18}O$ buffering.

Third, ISOLUTION treats the rate-limiting CO_2 hydration/HCO_3^- dehydroxylation step as occurring in isotope equilibrium but chemical disequilibrium, neglecting to explicitly model KIE during this step. KIE associated with the CO_2 hydroxylation/HCO_3^- dehydroxylation step are expected to yield fractionation factors smaller than expected for isotope equilibrium fractionation (McConnaughey, 1989; Clark et al., 1992; Devriendt et al., 2017). In ISOLUTION, because the bulk oxygen isotope fractionation factor between HCO_3^- and all reaction products depends on the calcite-water oxygen isotope fractionation factor chosen (See Table 1: G1, G2, G3), the overall effect of neglecting to model KIE also depends on the choice of calcite-water oxygen isotope fractionation factor. Each of the calcite-water oxygen isotope "equilibrium" fractionation factors chosen here includes a degree of KIE during CO_2 (de)hydroxylation/HCO_3^- (de)hydroxylation and underestimates true equilibrium values, with the possible exception of the Coplen (2007) calibration (Daëron et al., 2019). By basing ISOLUTION off one of these calibrations, ISOLUTION implicitly assumes that the direction and magnitude of KIE in the modeled system are similar to those in the experimental setup from which the equilibrium fractionation factors were calculated. Although this is not an ideal situation, it likely moderates the drawbacks of neglecting to explicitly model KIE in ISOLUTION.

Fourth, the ISOLUTION model takes a naïve approach to the speciation of DIC in solution and assumes that all calcite precipitation occurs in equilibrium with $HCO_{3(aq)}$, which is in turn in equilibrium with other DIC species. Because either carbonate or bicarbonate ions can attach to the calcite crystal surface, the pH-dependence of DIC speciation adds a slight pH dependence to calcite-water oxygen isotope fractionation (Watkins et al., 2013) that is unaccounted for by ISOLUTION. At the pH ranges observed at Jinapsan cave (6.61–8.57), however, $HCO_{3(aq)}$ comprises 67–98% of the DIC in solution. If the low outlier pH value is removed, the remaining pH values (7.76–8.57) correspond to a DIC pool composed of 96–98% $HCO_{3(aq)}$, suggesting that pH dependence is not significant at Jinapsan cave. This may not be the case at drip sites with more variable chemical compositions. Given the broad agreement between the modeled and measured calcite $\delta^{18}O$ values at drip site Stumpy (and to a lesser extent, Stations 1 and 2), we interpret this to mean that these four unmodeled effects are, in combination, relatively insignificant compared to the effects of Rayleigh fractionation at Jinapsan Cave, especially over seasonal timescales.

5.7. Implications for paleoclimate reconstruction

Although the importance of isotope disequilibrium fractionation to speleothem $\delta^{18}O$ values has been recently challenged (Dreybrodt & Scholz, 2011; Dreybrodt, 2016; Dreybrodt & Romanov, 2016), we find that at sites with slow drips and extended periods with high and low cave-air CO_2, isotope disequilibrium fractionation can account for temperature-independent shifts in $\Delta^{18}O_{c-w}$ values of 1–2‰. Shifts of this magnitude in a speleothem oxygen isotope records could be otherwise interpreted as a 5–10 °C swing in temperatures or a significant change in rainfall $\delta^{18}O$ values. This is consistent with Deininger and Scholz (2019), where independently-varied drip interval, cave air pCO_2, and drip water pCO_2 were each found to result in ISOLUTION-modeled calcite $\delta^{18}O$ values that varied on the order of up to 1‰ at long drip intervals, with the strongest controls exerted by drip rate and cave air pCO_2. Neglecting the effects of either could result in underestimating paleotemperatures by up to 5 °C. Neglecting the combined effects of drip interval, cave air pCO_2, and drip water pCO_2 could explain the larger offsets observed in this study.

Accounting for isotope disequilibrium fractionation on the surface of the speleothem could therefore provide additional hypotheses to explain shifts within speleothem $\delta^{18}O$ timeseries. Furthermore, a variably ventilated chamber, such as the Stumpy site, is not an optimal location to look for a speleothem to reconstruct climate due to degree of isotope disequilibrium fractionation, especially at a site with a slow drip rate where the effect is magnified.

Because the degree of Rayleigh fractionation is controlled by multiple variables, the paleoenvironmental importance of disequilibrium fractionation is unclear. The extent of disequilibrium fractionation could be modulated by increasing and decreasing drip rates, changes in cave ventilation due to cave burial, exhumation, or collapse, or due to changes in land surface cover altering subsurface CO_2 concentrations. Interpreting the root causes behind signals in a speleothem record likely require multiproxy records and a comparative analysis of coeval and co-located speleothems with different drip rates.

The observation of CO_2-driven seasonality in calcite $\delta^{18}O$ values also suggests the possibility of a new mechanism for $\delta^{18}O$ cycle chronometry in certain high-resolution speleothem records. Although cyclical $\delta^{18}O$ records have been used to inform speleothem chronologies before, these cycles have previously been driven by changes in precipitation $\delta^{18}O$ values (e.g., Treble et al., 2005; Johnson et al., 2006; Orland et al., 2015), or seasonal changes in cave air temperature (e.g., Feng et al., 2014; Carlson et al., 2018). As many caves in temperate regions are seasonally ventilated (Wigley and Brown, 1976; Buecher, 1999; James et al., 2015), regular CO_2-driven calcite $\delta^{18}O$ cycles may provide additional chronological constraints where drip rates are low, calcite growth is

year-round, and seasonal changes in cave temperature or drip $\delta^{18}O$ are not significant.

6. CONCLUSIONS

Through a combination of proxy system modelling and cave monitoring, we show that models that include isotope disequilibrium fractionation through Rayleigh fractionation can explain seasonal variations in calcite-water oxygen isotope fractionation at slow and moderate drip-rate sites. This control is exerted most significantly in speleothems with slow and consistent drip rates in variably ventilated chambers that experience large, seasonal CO_2 change. Although this process has been extensively modeled, its importance in speleothem oxygen isotope records has been debated. Through the mechanism of CO_2 degassing driving Rayleigh fractionation, seasonal CO_2 variations can account for variation in oxygen isotope fractionation factors at a slow drip-rate site in Jinapsan Cave, Guam. This is the first time that CO_2 concentrations have been observed as a primary control on cave calcite oxygen isotope variability. Although this control is less dominant at better ventilated and faster or more variable drip-rate sites in Jinapsan Cave, this finding provides important context to interpretations of slow drip-rate speleothem records.

Declaration of Competing Interest

The authors declare that they have no known competing financial interests or personal relationships that could have appeared to influence the work reported in this paper.

ACKNOWLEDGEMENTS

Funding for this research was provided by the Strategic Environmental Research and Development Program (SERDP Project Number 13 RC01–004/RC–2340), and the Pacific Islands Climate Science Center (G12AC0003). This research was also supported by National Science Foundation grants awarded to J. Gulley, D. Breecker, and J. Banner (EAR-1452024), and to J. Partin, J. Jenson, and J. Banner (AGS-1003700). B. Hardt provided early input in designing this study and organizing its associated field campaigns. Travel and other support provided by the University of Texas at Austin College of Natural Sciences, Environmental Science Institute, Geology Foundation F. M. Bullard Professorship, and Planet Texas 2050 initiative.

Modified ISOLUTION code, data processing code, and statistical analysis code can be accessed at github.com/PeterECarlson/GuamOxygenIsotopes.

APPENDIX A. SUPPLEMENTARY MATERIAL

Supplementary data to this article can be found online at https://doi.org/10.1016/j.gca.2020.06.012.

REFERENCES

Affek H. P. and Zaarur S. (2014) Kinetic isotope effect in CO2 degassing: insight from clumped and oxygen isotopes in laboratory precipitation experiments. *Geochim. Cosmochim. Acta* **143**, 319–330.

Banner J. L., Guilfoyle A., James E. W., Stern L. A. and Musgrove M. (2007) Seasonal Variations in Modern Speleothem Calcite Growth in Central Texas, U.S.A. *J. Sediment. Res.* **77**(8), 615–622.

Bar-Matthews M., Ayalon A., Matthews A., Sass E. and Halicz L. (1996) Carbon and oxygen isotope study of the active water-carbonate system in a karstic Mediterranean cave: Implications for paleoclimate research in semiarid regions. *Geochim. Cosmochim. Acta* **60**, 337–347.

Bautista, K.K., Jensen, J.W., Lander, M., Righetti, T., 2018. Vadose Hydrology at Jinapsan Cave, Northern Guam. Water and Environmental Research Institute of the Western Pacific Technical Reports, 163.

Beal L., Wong C. I., Bautista K., Jenson J. W., Banner J. L., Lander M. A., Gingerich S. B., Partin J. W., Hardt B. and van Oort N. H. (2018) Isotopic and geochemical assessment of the sensitivity of groundwater resources of Guam, Mariana Islands, to intra- and inter-annual variations in hydroclimate. *J. Hydrol.* **568**, 174–183.

Beck W., Grossman E. and Morse J. (2005) Experimental studies of oxygen isotope fractionation in the carbonic acid system at 15°, 25° and 40°C. *Geochim. Cosmochim. Acta* **69**, 3493–3503.

Buecher R. (1999) Microclimate study of Kartchner Caverns, Arizona. *J. Cave Karst Stud.* **61**, 108–120.

Carlson P. E., Miller N. R., Banner J. L., Breecker D. O. and Casteel R. C. (2018) Subannually resolved speleothem chronology in a near-entrance cave setting using oxygen isotope and trace element variations driven by temperature seasonality. *Geochim. Cosmochim. Acta.* **235**, 55–75.

Chacko T. and Deines P. (2008) Theoretical calculation of oxygen isotope fractionation factors in carbonate systems. *Geochim. et Cosmochim. Acta* **72**, 3642–3660.

Chen S., Gagnon A. C. and Adkins J. F. (2018) Carbonic anhydrase, coral calcification and a new model of stable isotope vital effects. *Geochim. et Cosmochim. Acta.* **236**, 179–197.

Clark I. D., Fontes J.-C. and Fritz P. (1992) Stable isotope disequilibria in travertine from high pH waters: laboratory investigations and field observations from Oman. *Geochim. et Cosmochim. Acta* **56**, 2041–2050.

Coplen T. B. (2007) Calibration of the calcite-water oxygen-isotope geothermometer at Devils Hole, Nevada, a natural laboratory. *Geochim. Cosmochim. Acta* **71**, 3948–3957.

Daëron M., Drysdale R. N., Peral M., DHuyghe D., Blamart D., Coplen T. B., Lartaud F. and Zanchetta G. (2019) Most Earth-surface calcites precipitate out of isotopic equilibrium. *Nature Comm.* **10**, 429.

Day C. C. and Henderson G. M. (2011) Oxygen isotopes in calcite grown under cave-analogue conditions. *Geochim. Cosmochim. Acta* **75**(14), 3956–3972.

Deininger M., Fohlmeister J., Scholz D. and Mangini A. (2012) Isotope disequilibrium effects: the influence of evaporation and ventilation effects on the carbon and oxygen isotope composition of speleothems—A model approach. *Geochim. Cosmochim. Acta* **96**, 57–79.

Deininger M. and Scholz D. (2019) ISOLUTION 1.0: an ISOtope evoLUTION model describing the stable oxygen ($\delta^{18}O$) and carbon ($\delta^{13}C$) isotope values of speleothems. *Int. J. of Speleology* **48**(1).

DePaolo D. J. (2011) Surface kinetic model for isotopic and trace element fractionation during precipitation of calcite from aqueous solutions. *Geochim. Cosmochim. Acta* **75**(4), 1039–1056.

Desmarchelier J. M., Goede A., Ayliffe L. K., McCulloch M. T. and Moriarty K. (2000) Stable isotope record and its paleoenvironmental interpretation for a late Middle Pleistocene speleothem from Victoria Fossil Cave, Naracoorte, South Australia. *Quat. Sci. Rev.* **19**, 763–774.

Dietzel M., Tang J., Leis A. and Köhler S. J. (2009) Oxygen isotopic fractionation during inorganic calcite precipitation - Effects of temperature, precipitation rate and pH. *Chem. Geol.* **208**, 107–115.

Devriendt L. S., Watkins J. M. and McGregor H. V. (2017) Oxygen isotope fractionation in the $CaCO_3$-DIC-H_2O system. *Geochim. et Cosmochim. Acta* **214**, 115–142.

Donnegan J. A., Butler S. A., Grabowiecki W., Hiserote B. A. and Limtiaco D. (2004) *Guam's Forest Resources, 2002. Resour. Bull. PNW-RB-243*. U.S. Department of Agriculture, Forest Service, Pacific Northwest Research Station, Portland, OR, p. 32.

Dreybrodt W. (2008) Evolution of the isotopic composition of carbon and oxygen in a calcite precipitating H_20-CO_2-$CaCO_3$ solution and the related isotopic composition of calcite in stalagmites. *Geochim. Cosmochim. Acta* **72**(19), 4712–4724.

Dreybrodt W. (2016) Problems in using the approach of Rayleigh distillation to interpret the ^{13}C and ^{18}O isotope compositions in stalagmite calcite. *Acta Carsologica* **45**(3), 287–293.

Dreybrodt W., Eisenlohr B., Madry B. and Ringer S. (1998) Precipitation kinetics of calcite in the system CaCO3-H2O-CO2: The conversion to CO_2 by the slow process $H^+ + HCO_3^- \rightarrow CO_2 + H_2O$ and the inhibition of surface controlled reactions as rate limiting steps. *Geochim. Cosmochim. Acta* **61** (18), 3897–3904.

Dreybrodt W., Hansen M. and Scholz D. (2016) Processes affecting the stable isotope composition of calcite during precipitation on the surface of stalagmites: Laboratory experiments investigating the isotope exchange between DIC in the solution layer on top of a speleothem and the CO_2 of the cave atmosphere. *Geochim. Et Cosmochim. Acta* **174**, 247–262.

Dreybrodt W. and Romanov D. (2016) The evolution of ^{13}C and ^{18}O isotope composition of DIC in a calcite depositing film of water with isotope exchange between the DIC and a CO_2 containing atmosphere, and simultaneous evaporation of the water. Implication to climate proxies from stalagmites: A theoretical model. *Geochim. Cosmochim. Acta* **195**, 323–338.

Dreybrodt W. and Scholz D. (2011) Climatic dependence of stable carbon and oxygen isotope signals recorded in speleothems: From soil water to speleothem calcite. *Geochim. Cosmochim. Acta* **75**(3), 734–752.

Feng W., Banner J. L., Guilfoyle A. L., Musgrove M. and James E. W. (2012) Oxygen isotopic fractionation between drip water and speleothem calcite: A 10-year monitoring study, central Texas, USA. *Chem. Geol.* **305**, 53–67.

Feng W., Casteel R. C., Banner J. L. and Heinze-Fry A. (2014) Oxygen isotope variations in rainfall, drip-water and speleothem calcite from a well-ventilated cave in Texas, USA: Assessing a new speleothem temperature proxy. *Geochim. Cosmochim. Ac.* **125**, 233–250.

Friedman I. and O'Neil J. R. (1977) *Compilation of isotopic fractionation factors of geochemical interest*. U.S. Geological Survey Professional Paper. 440-KK.

Gabitov R. I., Watson E. B. and Sadekov A. (2012) Oxygen isotope fractionation between calcite and fluid as a function of growth rate and temperature: An in situ study. *Chem. Geol.* **306–307**, 92–102.

Granit N. F., Korin E. and Bettelheim A. (2003) Effect of Organic Additives on Electrochemical Surface Precipitation and Polymorphism of $CaCO_3$. *Chem. Eng. and Tech.* **26**(3), 341–346.

Guo W. and Zhou C. (2019) Patterns and controls of disequilibrium isotope effects in speleothems: Insights from an isotope-enabled diffusion-reaction model and implications for quantitative thermometry. *Geochim. et Cosmochim. Acta.* **267**, 196–226.

Hansen M., Dreybrodt W. and Scholz D. (2013) Chemical evolution of dissolved inorganic carbon species flowing in thin water films and its implications for (rapid) degassing of CO_2 during speleothem growth. *Gheochim. Cosmochim. Acta* **207**, 242–251.

Hansen M., Scholz D., Schöne B. R. and Spötl C. (2019) Simulating speleothem growth in the laboratory: Determination of the stable isotope fractionation ($\delta^{13}C$ and $\delta^{18}O$) between H_2O, DIC, and $CaCO_3$. *Chem. Geol.* **509**, 20–44.

Hendy C. H. (1971) The isotopic geochemistry of speleothemsI. The calculation of the effects of different modes of formation on the isotopic composition of speleothems and their applicability as palaeoclimatic indicators. *Geochim. Cosmochim. Acta.* **35**, 801–824.

Hu J., Emile-Geay J. and Partin J. (2017) Correlation-based interpretations of paleoclimate data—where statistics meet past climates. *Earth and Plan. Sci. Let.* **459**, 362–371.

Ihli J., Clark J. N., Côté A. S., Kim Y.-Y., Schenk A. S., Kulak A. N., Comyn T. P., Chammas O., Harder R. J., Duffy D. M., Robinson I. K. and Meldrum F. C. (2016) Strain-relief by single dislocation loops in calcite crystals grown on self-assembled monolayers. *Nature Comm.* **7**, 11878.

Innocenti Malini R., Finney A. R., Hall S. A., Freeman C. L. and Harding J. H. (2017) The Water-Amorphous Calcium Carbonate Interface and Its Interactions with Amino Acids. *Cryst. Growth Des.* **17**(11), 5811–5822.

Inskeep W. P. and Bloom P. R. (1986) Kinetics of calcite precipitation in the presence of water-soluble organic ligands. *Soil Sci. Soc. Am. J.* **50**, 1167–1172.

James E. W., Banner J. L. and Hardt B. (2015) A global model for cave ventilation and seasonal bias in speleothem paleoclimate records. *Geochem. Geophys. Geosyst.* **16**(4), 1044–1051.

Johnson K. R., Hu C., Belshaw N. S. and Henderson G. M. (2006) Seasonal trace-element and stable-isotope variations in a Chinese speleothem: the potential for highresolution paleomonsoon reconstruction. *Earth Planet. Sc. Lett.* **244**, 394–407.

Johnston V. E., Borsato A., Spötl C., Frisia S. and Miorandi R. (2013) Stable isotopes in caves over altitudinal gradients: fractionation behaviour and inferences for speleothem sensitivity to climate change. *Clim. Past* **9**(1), 99–118.

Kim S.-T. and O'Neil J. R. (1997) Equilibrium and nonequilibrium oxygen isotope effects in synthetic carbonates. *Geochim. Cosmochim. Acta* **61**(16), 3461–3475.

Kim S.-T., Hillaire-Marcel C. and Mucci A. (2006) Mechanisms of equilibrium and kinetic oxygen isotope effects in synthetic aragonite at 25 °C. *Geochim. et Cosmochim. Acta* **70**, 5790–5801.

Kubota H. and Wang B. (2009) How much do tropical cyclones affect seasonal and interannual rainfall variability over the western North Pacific? *J. Clim.* **22**(20), 5495–5510.

Lander, M. A. and Guard, C. P. (2003) Creation of a 50-Year Rainfall Database, Annual Rainfall Climatology and Annual Rainfall Distribution Map for Guam. Forecast (102).

Lander, M. A., Jenson, J. W. and Beausoliel, C. (2001) Responses of Well Water Levels on Northern Guam to Variations of Rainfall and Sea Level. Tech. rep.

Levitt N. P., Eiler J. M., Romanek C. S., Beard B. L., Xu H. and Johnson C. M. (2018) Near equilibrium ^{13}C–^{18}O bonding

during inorganic calcite precipitation under chemo-stat conditions. *Geochem. Geophys. Geosyst.* **19**, 901–920. https://doi.org/10.1002/2017GC007089.

McConnaughey T. (1989) ^{13}C and ^{18}O isotopic disequilibrium in biological carbonates: II. In vitro simulation of kinetic isotope effects. *Geochim. Cosmochim. Acta* **53**, 163–171.

McCrea J. M. (1950) On the isotopic chemistry of carbonates and a paleotemperature scale. *J. Chem. Phys.* **18** 849857.

McDermott F., Schwarcz H. and Rowe P. J. (2006) Isotopes in speleothems. In *Isotopes in Paleoenvironmental Research* (ed. M. J. Leng). Springer, Dordrecht, pp. 185–225.

McDermott F., Atkinson T., Fairchild I. J., Baldini L. M. and Mattey D. P. (2011) A first evaluation of the spatial gradients in $\delta^{18}O$ recorded by European Holocene speleothems. *Global Planet. Change* **79**(3–4), 275–287.

Mickler P. J., Banner J. L., Stern L., Asmerom Y., Edwards R. L. and Ito E. (2004) Stable isotope variations in modern tropical speleothems: Evaluating equilibrium vs. kinetic isotope effects. *Geochim. Cosmochim. Acta* **68**(21), 4381–4393.

Mickler P. J., Stern L. A. and Banner J. L. (2006) Large kinetic isotope effects in modern speleothems. *Bulletin of the Geological Society of America* **118**(1), 65–81.

Mickler P. J., Carlson P. E., Banner J. L., Breecker D. O., Stern L. and Guilfoyle A. (2019) Quantifying carbon isotope disequilibrium during in-cave evolution of drip water along discreet flow paths. *Geochim. Cosmochim. Acta* **244**, 182–196.

Miklavič, B. (2011) Formation of geomorphic features as a response to sea-level change at Ritidian Point, Guam, Mariana. MS thesis. Dep. of Geosci., Miss. State Univ., Starkville.

Mühlinghaus C., Scholz D. and Mangini A. (2007) Modelling stalagmite growth and $\delta^{13}C$ as a function of drip interval and temperature. *Geochim. Cosmochim. Acta* **71**(11), 2780–2790.

Noronha A. L., Hardt B. F., Banner J. L., Jenson J. W., Partin J. W., James E. J., Lander M. A. and Bautista K. K. (2017) Trade winds drive pronounced seasonality in carbonate chemistry in a tropical Western Pacific island cave-Implications for speleothem paleoclimatology. *Geochem. Geophys. Geosyst.* **18**. https://doi.org/10.1002/2016GC006644.

O'Neil J. R., Clayton R. N. and Mayeda T. K. (1969) Oxygen isotope fractionation in divalent metal carbonates. *J. Chem. Phys.* **51**, 5547–5558.

Orland I. J., Edwards R. L., Cheng H., Kozdon R., Cross M. and Valley J. W. (2015) Direct measurements of deglacial monsoon strength in a Chinese stalagmite. *Geology* **43**, 555–558.

Owen R., Day C. C. and Henderson G. M. (2018) CaveCalc: A new model for speleothem chemistry and isotopes. *Comput. Geosci.* **119**, 115–122.

Parkhurst D. L. and Appelo C. A. J. (1999) *Users's guide to PHREEQC (Version 2) – a computer program for speciation, batch-reaction, one-dimensional transport, and inverse geochemical calculations* Water-Resources Investigations Report 99-4259. U.S. Geological Survey.

Partin J. W., Jenson J. W., Banner J. L., Quinn T. M., Taylor F. W., Sinclair D. J., Hardt B., Lander M. A., Bell T., Miklavič B., Jocson J. M. U. and Taborŏsi D. (2012) Relationship between modern rainfall variability, cave dripwater, and stalagmite geochemistry in Guam, USA. *Geochem. Geophys. Geosyst.* **13** (3), Q03013.

Polag D., Scholz D., Mühlinghaus C., Spötl C., Schröder-Ritzrau A., Segl M. and Mangini A. (2010) Stable isotope fractionation in speleothems: Laboratory experiments. *Chem. Geol.* **279**(1–2), 31–39.

Romanov D., Kaufmann G. and Dreybrodt W. (2008) $\delta^{13}C$ profiles along growth layers of stalagmites: comparing theoretical and experimental results. *Geochim. et Cosmochim. Acta* **72**, 438–448.

Sade Z. and Halevy I. (2017) New constraints on kinetic isotope effects during $CO_{2(aq)}$ hydration and hydroxylation: Revisiting theoretical and experimental data. *Geochim. et Cosmochim. Acta.* **214**, 246–265.

Sinclair D. J., Banner J. L., Taylor F. W., Partin J. W., Jenson J., Mylroie J., Goddard E., Quinn T., Jocson J. and Miklavič B. (2012) Magnesium and strontium systematics in tropical speleothems from the Western Pacific. *Chem. Geol.* **294–295**, 1–17.

Stoll H. M., Mendez-Vicente A., Gonzalez-Lemos S., Moreno A., Cacho I., Cheng H. and Edwards R. L. (2015) Interpretation of orbital scale variability in mid-latitude speleothem $\delta^{18}O$: Significance of growth rate controlled kinetic fractionation effects. *Quat. Sci. Rev.*, 1–14.

Tang H., Xian H., He H., Wei J., Liu H., Zhu J. and Zhu R. (2019) Kinetics and mechanisms of the interaction between the calcite (10.4) surface and Cu2+-bearing solutions. *Sci. Tot. Env.* **668**, 602–616.

Thorstenson D. and Parkhurst D. (2004) Calculation of individual equilibrium constants for geochemical reactions. *Geochim. Cosmochim. Acta* **68**, 2449–2465.

Treble P. C., Chappell J., Gagan M. K., McKeegan K. D. and Harrison T. M. (2005) In situ measurement of seasonal δ18O variations and analysis of isotopic trends in a modern speleothem from southwest Australia. *Earth Planet. Sci. Lett.* **233**, 1732.

Tremaine D. M., Froelich P. N. and Wang Y. (2011) Speleothem calcite farmed in situ: Modern calibration of $\delta^{18}O$ and $\delta^{13}C$ paleoclimate proxies in a continuously-monitored natural cave system. *Geochim. Cosmochim. Acta* **75**, 4929–4950.

Urey H. C. (1947) The thermodynamic properties of isotopic substances. *J. Chem. Soc.*, 562–581.

Watkins J. M., Nielsen L., Ryerson F. and DePaolo D. J. (2013) The influence of kinetics on the oxygen isotope composition of calcium carbonate. *Earth Planet. Sci. Lett.* **375**, 349–360.

Watkins J. M., Hunt J. D., Ryerson F. J. and DePaolo D. J. (2014) The influence of temperature, pH, and growth rate on the $\delta^{18}O$ composition of inorganically precipitated calcite. *Earth Planet. Sci. Lett.* **404**, 332–343.

Watson E. B. (1996) Surface enrichment and trace-element uptake during crystal growth. *Geochim. Cosmochim. Acta* **60**, 5013–5020.

Watson E. B. (2004) A conceptual model for near-surface kinetic controls on the trace- element and stable isotope composition of abiogenic calcite crystals. *Geochim. Cosmochim. Acta* **68**(7), 1473–1488.

Watson E. B. and Liang Y. (1995) A simple model for sector zoning in slowly grown crystals: implications for growth rate and lattice diffusion, with emphasis on accessory minerals in crustal rocks. *Am. Mineral.* **80**, 1179–1187.

Wigley T. M. L. and Brown M. C. (1976) The physics of caves. In *The Science of Speleology*, vol. 3 (eds. T. D. Ford and C. H. D. Cullingford). Academic, N. Y., pp. 329–347.

Zhang P., Johnson K. R., Chen Y., Chen F., Ingram L., Zhang X., Zhang C., Wang S., Pang F. and Long L. (2004) Modern systematics and environmental significance of stable isotopic variations in Wanxiang Cave, Wudu, Gansu. *China. Chinese Sci. Bull.* **49**, 1649–1652.

Associate editor: Jay Quade